IISc Theses Abstracts

Contents

J. Indian Inst. Sci., Jan.–Feb. 1996, 76, 127–157.

IISc THESES ABSTRACTS

Thesis Abstract (Ph. D.)

Phasons, topological defects and dynamics in incommensurate matter by Yashodhan Vinod Kumar Hatwalne

Research supervisors: Sriram Ramaswamy and T. V. Ramakrishnan
Department: Physics

1. Introduction

In this thesis we derive some physical consequences of the existence of a phason mode in incommensurate materials by considering two examples—quasicrystals and the incommensurate twist grain boundary (i-TGB) phase of liquid crystals.

The three principal results on quasicrystals are: an elucidation of the structure of small-angle grain boundaries, a method for determining the full six-dimensional Burgers vector for quasicrystal dislocations from diffraction contrast, and new predictions which allow a detailed test of the entropic model of quasicrystals.

For the i-TGB phase, we present results on the nature of the broken symmetry, linear and nonlinear elasticity and hydrodynamics, including the effects of thermal fluctuations.

In Chapter I we describe the structure of quasicrystals and the i-TGB phase. We identify the broken symmetry variables in quasicrystals using the Landau theory and briefly review the earlier work on continuum elasticity theory and dislocations in quasicrystals. We also give a physical picture of the diffusive nature of phason dynamics.

2. Results

Chapter II contains a derivation of 'invisibility condition' for transmission electron micrographs of dislocation in quasicrystals using the density-wave framework. We show why this condition is essential for a complete analysis of quasicrystal dislocations[1].

In Chapter III, we generalize Frank's formula for the dislocation content of small-angle grain boundaries in crystals, and the Read–Shockley treatment of small-angle grain boundaries in crystals to the case of quasicrystals. We find that even for a symmetric tilt boundary, dislocations with at least two types of Burgers vectors are required; these dislocations have to be arranged quasiperiodically along the boundary. We calculate the dependence of the grain boundary on the angle of mismatch and discuss the possible clumping of dislocations to form composites[2].

In Chapter IV, we describe the entropic model of quasicrystals and show how it leads to a square-gradient elastic-free energy in the phason variable. We give an intuitively appealing demonstration showing that the free energy of a dislocation line is logarithmic in the system size within this model. Assuming the validity of this model, we derive prediction for the temperature dependence of the grain boundary structure and free energy, the nature of the elastic instability, and the behaviour of sound damping near this instability. We believe that these predictions will provide decisive tests for the entropic model of quasicrystals[3].

A simple analysis of Griffith cracks in quasicrystals is presented in Chapter V. We obtain the expression for critical crack length and show how this could be used as a test for the entropic model, in addition to the tests proposed in Chapter IV.

In Chapter VI, we consider a model of the i-TGB phase in which dislocation lines are not ordered within any grain boundary. We study the nature of the broken continuous symmetry and set up the nonlinear, continuum elasticity theory of this phase form symmetry considerations. Using a perturbative, momentum-shell renormalization group treatment, we show how thermal fluctuations and nonlinearities in the elastic Hamiltonian yield elastic constants that depend logarithmically on the length scale. We then study the dynamics of this phase by setting up the generalized Langenvin equations and obtain the linear mode structure. We also study the effects of out-of-plane fluctuations of the grain boundaries on the viscosity to show that certain components of the viscosity tensor diverge at small frequencies.

References

1. HATWALNE, Y. AND RAMASWAMY, S. *Phil. Mag. Lett.*, 1990, **61**, 169.

2. HATWALNE, Y., KRISHNAMURTHY, H. R., PANDIT, R. AND RAMASWAMY, S. *Phys. Rev. Lett.*, 1989, **62**, 2699.

3. HATWALNE, Y. AND RAMASWAMY, S. *Phys. Rev. Lett.*, 1990, **65**, 68.

Thesis Abstract (Ph. D.)

Ion assisted deposition of CeO_2 and Al_2O_3 films by Mansour Suckar Farhan

Research supervisors: S. Mohan and K. Narasimha Rao

Department: Instrumentation and Services Unit

1. Introduction

Novel deposition techniques and new materials are two very important aspects in the development of optical thin film devices. Hence, they have received a lot of attention right through the development of the science and technology of thin films. Although dielectric oxides constitute only a very small percentage of the materials used for optical devices, they have proved to be much superior to numerous other materials by virtue of their hardness, durability, refraction index, low extinction coefficient, etc. They have the additional advantage that with a proper selection of deposition process and process parameters the above-mentioned properties can be tailored to suit specific applications.

A number of physical vapour deposition techniques have been used to deposit oxide thin films. But better control over the properties has been achieved only by the use of ion-assisted deposition processes. This is a consequence of the simple manner in which ion source parameters can be controlled to obtain the desired properties[1-5].

The objective of the present work is to study the variation in properties of ceria and alumina thin films deposited by ion-assisted deposition electron beam evaporation using oxygen and argon ions.

2. Experimental procedure

The films were prepared in an oil diffusion pumped chamber which could give pressures of the order of 5×10^{-6} mbar. The films were coated on fused silica substrates. The source to distance

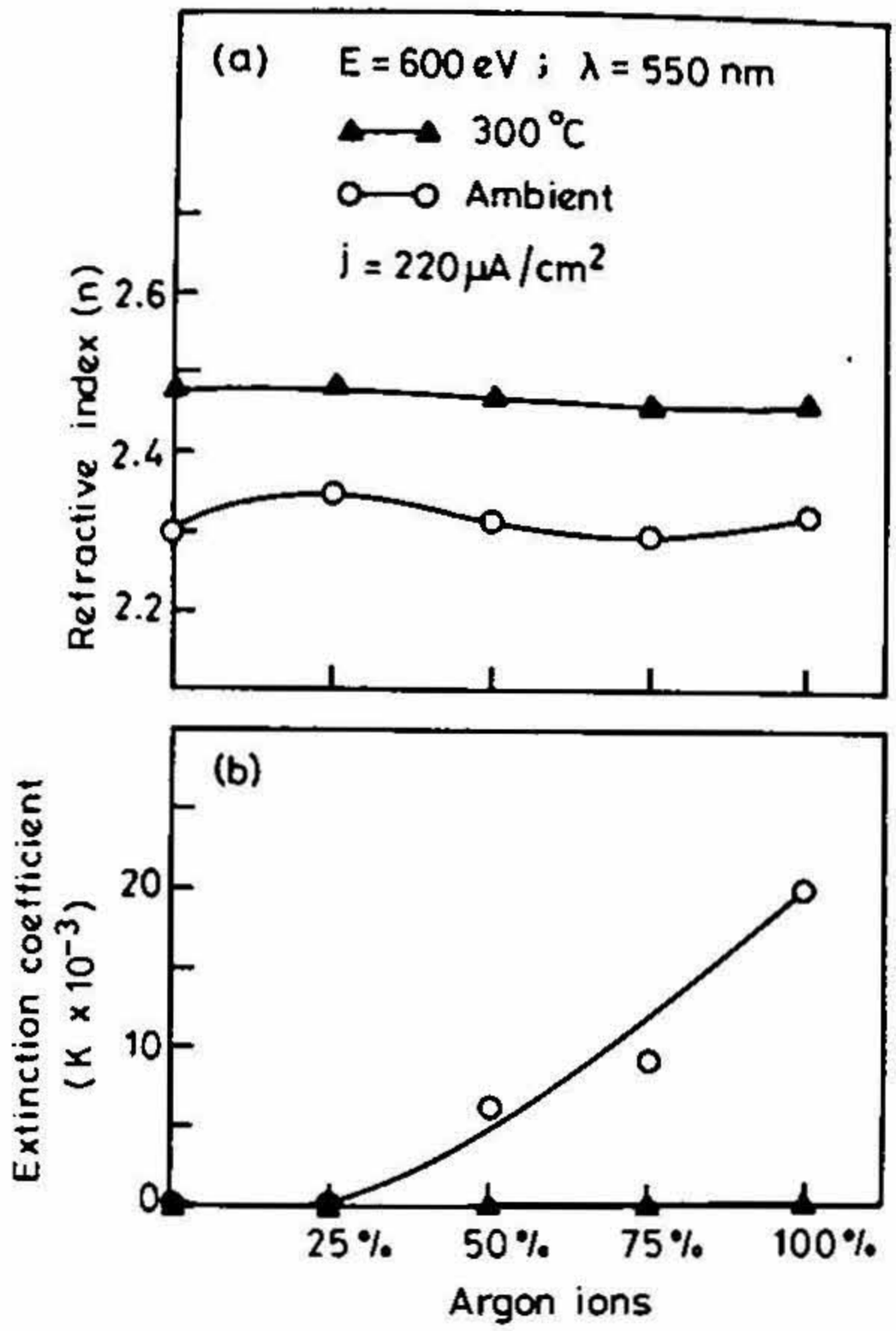

FIG. 1. Variation in (a) refractive index and (b) extinction coefficient as a function of argon ion percentage.

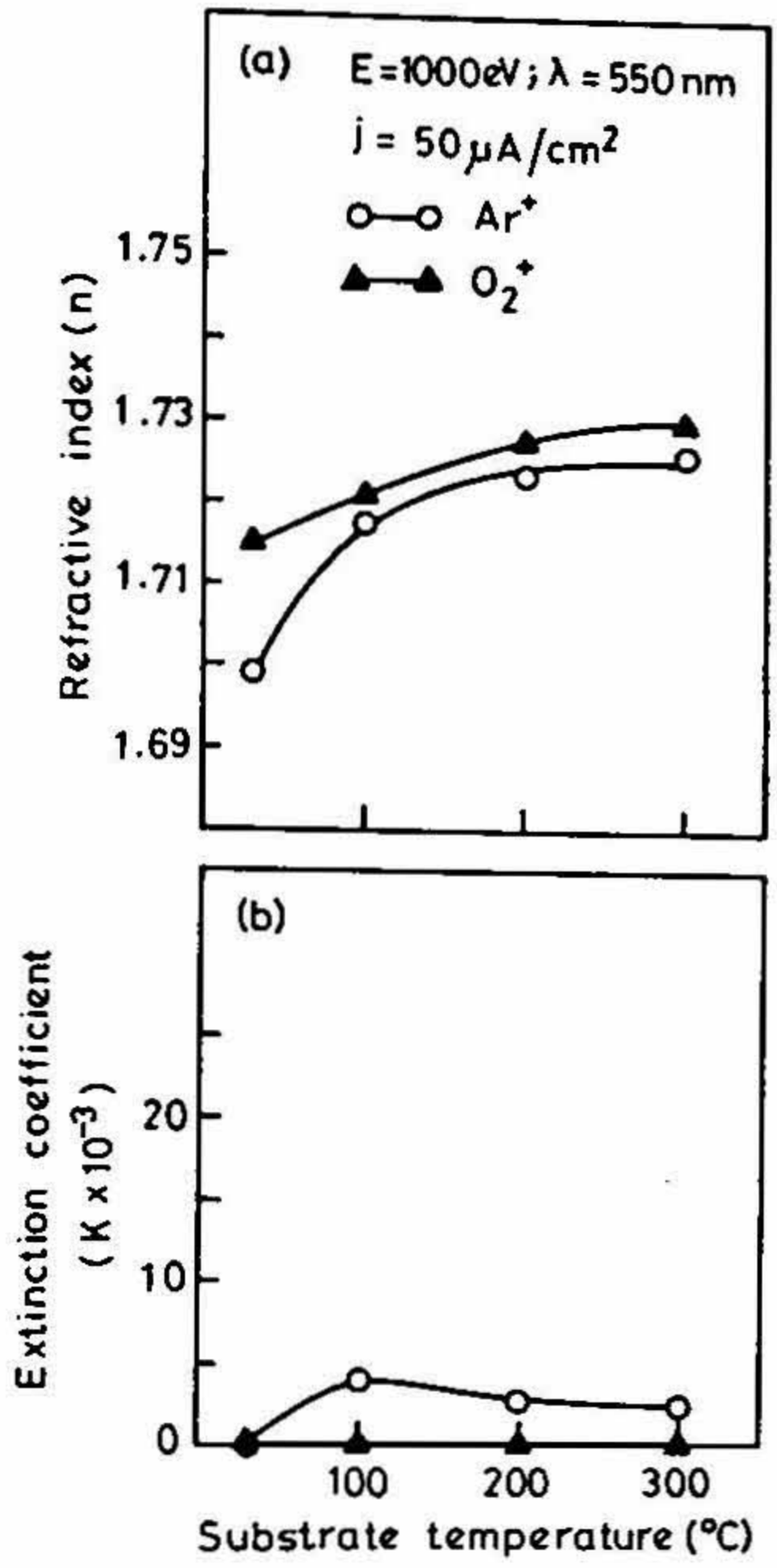

FIG. 2. Variation in (a) refractive index and (b) extinction coefficient as a function of substrate temperature.

was 28 cm. Ceria and alumina films were coated usi[ng] respectively, CeO_2 and Al_2O_3 as starting materials. Substrates were heated during deposition [us]ing a radiant heater. Oxygen and argon ions were produced using a broad beam high-energy [Kau]fman-type ion source. This can produce ions of energy up to 1500 eV and current up to 1[A]. The films were characterized for the following properties: refractive index, extinction coe[f]ficient, packing density and structure.

Ceria and alumina thin films were deposited at i[on] energy range up to 1000 eV, current densities up to 220 $\mu A/cm^2$ and substrate temperature up [to] 300°C. The starting material was evaporated from an electron beam source. The upper value [for] ion energy and current density were set by the deterioration in optical properties.

3. Results and conclusions

The major results of the work have been summarized in Figs 1 and 2. The combined effect of substrate temperature and Ar^+/O^+ ion beam parameters on the properties of CeO_2 films has been shown in Figs 1a–b. Figure 1a represents the refractive index variation with argon ion percentage for films deposited with ions of energy 600 eV, current density of 220 $\mu A/cm^2$, at

maintained and 300° C substrate temperatures. The refractive index at 300° C substrate temperature reached the bulk-like index value ($n = 2.48$) for all values of argon percentage. The above observations can be explained on the basis that the additional energy imparted, by both the substrate temperature and ion beams, to adatom resulted in modification of the film microstructure and leads to increase in packing density. This value can be compared favourably with that reported by Netterfield *et al*[5].

Figure 1b represents the extinction coefficient variation as a function of argon ion percentage for these films. It was observed that the extinction coefficient values increased with increase in argon ion percentage at ambient substrate temperature. However, at 300° C substrate temperature, the extinction coefficient was negligibly small whatever be the argon ion percentage.

The combined influence of substrate temperature and ion beam parameters on the properties of Al_2O_3 films deposited with oxygen and argon ion bombardment at 1000 eV and at ion-to-atom arrival ratio of 0.45, the refractive index and extinction coefficient as a function of substrate temperature are plotted in Figs 2a–b. The refractive indices at elevated substrate temperature were found to be high and the same regardless of ion beam species. The argon ion bombarded films showed decrease in the extinction coefficient as the substrate temperature increased in contrast to the films deposited using oxygen ion-assisted deposition.

From these observations, transparent CeO_2 and Al_2O_3 films with bulk-like refractive indices and packing densities of approximately unity can be obtained by depositing them either by using oxygen or argon IAD.

References

1. Martin, P. J. — *Vacuum*, 1986, **36**, 585.
2. Martin, P. J. and Netterfield, R. P. — *Thin solid films*, 1991, **199**, 35.
3. Mcnally, J. J. — Ph. D. Thesis, University of New Mexico, 1986.
4. Targove, J. D. and Macleod, H. A. — *Appl. Opt.*, 1988, **27**, 3779.
5. Netterfield, R. P., Sainty, W. G., Martin, P. J. and Sie, S. H. — *Appl. Opt.*, 1985, **24**, 2367.

Thesis Abstract (Ph. D.)

S-nets: A tool for the performance evaluation of hard real-time scheduling algorithms by S. Balaji

Research supervisors: Lawrence Jenkins, L. M. Patnaik and P. S. Goel

Department: Electrical Engineering

1. Introduction

The workloads of hard real-time systems (HRTSs) comprise predominantly periodic tasks[1]. In an HRTS, computations must satisfy critical time constraints. The system must be able to meet critical deadlines even when it suffers certain failures[2]. The complexity of real-time systems is growing rapidly, and the computers in these systems are so complex that a manual override of the computer for fault recovery is impossible. This is especially true in the aerospace field. The com-

puters used in these applications must be extremely robust, and must be capable of fast response times. An essential part of the development of real-time software is the process of verifying that real-time software meets its timing constraints, which is referred to as the worst case schedulability analysis, or simply schedulability analysis[3]. Due to the increasing number and sophistication of real-time applications, there is a growing need for tools for schedulability analysis. Schedulability analysis must take into account the specific fault-tolerance techniques used; for example, the deadline mechanism[4].

Another important aspect of designing real-time systems is the performance evaluation of the scheduling algorithms used for the distribution of the workload among the processors of the HRTS[5]. The emphasis in hard real-time scheduling is on developing scheduling algorithms which satisfy time constraints while maintaining a balanced distribution of workload among the processors. A number of algorithms may be used to schedule the workload and the results of the schedulability analysis may be used in arriving at a simple scheduling algorithm that guarantees deadlines and distributes the workload among the processing resources in a balanced fashion. In this work, a new Petri net-based tool is presented for an integrated analysis of schedulability and performance[6].

2. S-nets

The behaviour of the HRTSs is deterministic, except for the nondeterministic failure characteristics. Consequently, deterministic-timed Petri nets (DTPNs)[7], in which the transition firing times are deterministic, are used to analyse HRTSs. Although DTPNs support mechanisms to model conflicting events, these mechanisms are not adequate to model scheduling algorithms. Because resource scheduling is carried out deterministically, the techniques of modelling conflicts cannot be used for modelling resource scheduling. Hence, the arbitration of resources should be modelled through a deterministic scheduling strategy[8]. The DTPNs do not facilitate the modelling of a deterministic scheduling policy, and hence they must be modified to represent resource contention, and must be augmented with features to model scheduling algorithms. Further, the number of places and transitions, in the DTPN model of a hard real-time system, is prohibitively large, and the graph representation of this DTPN model is too cumbersome to implement in a convenient form easy to follow.

Because of the limitations of DTPNs, a class of Petri nets, called *S-nets* (S stands for schedular) is developed. S-nets are based on DTPNs and are augmented with new types of places, called resource and signal places, and scheduler block to facilitate modelling of scheduling algorithms. The tokens are coloured, and are classified into four types: *frame* tokens, *task* tokens, *resource* tokens, and *signal* tokens. The transition firing rules are defined. The concept of transition folding is used to reduce the number of places and transitions so as to get intuitively simple models of multiframe real-time systems. S-nets also provide facilities to model a scheduling algorithm as a black box. The heuristics used for scheduling the tasks of a multiframe real-time system is specified during the process of state-space generation. It is shown that the reachability graph of an S-net model is a semi-Markov chain[9], and that steady-state probabilities exist for this chain. Using sparse matrix techniques, the steady-state probability distribution of the semi-Markov chain is computed. The steady-state probability distribution is useful in computing performance measures of interest. A method is outlined to compute generic performance measures from the steady-state probability distribution of the semi-Markov chain.

Two performance measures, called *load index* and *balance index* are defined which characterize the resource utilization and the uniformity of workload distribution, respectively, and

which can be computed from the steady-state probability distribution of the embedded Markov chain of the S-net model. The utility of S-nets for evaluating heuristic-based scheduling algorithms is illustrated by considering 11 heuristics for scheduling a number of cases of real-time workload.

Techniques of schedulability analysis and performance evaluation using S-nets are based on reachability analysis, which is the process of generating the states of a model and exhaustively exploring whether a desired condition holds in these states. As the complexity of the system model increases, manual generation of the state space becomes more and more cumbersome. This is particularly the case with HRTSs, which operate in multiple time frames. Reachability analysis, which involves the construction of the reachability graph, is a notoriously hard work. When automated, execution of the state-space generation algorithm needs prohibitively long time and large memory. To make matters more difficult, the graph is often infinite, and it is not obvious whether the reachability graph is finite. However, we have shown that the reachability graph is finite in the case of an S-net model of an HRTS operating in multiple time frames. In spite of these difficulties, reachability analysis has very often been used to check user-defined probes which express the properties of the system. Exhaustive exploration of the state space is still attractive since the system designer usually wants a total system behaviour to be expressed in the state space to analyse the properties of the system.

A software package, called SnetSim which interactively accepts the specification of the S-net model and builds the reachability graph, has been developed. The process of state-space generation for an S-net model is discussed; list structure representation of the S-net and the reachability graph, and the procedure for the generation of the state space are outlined. The list structures required and the generic list processing involved in generating the state space of an S-net model have been presented. The state-space generation algorithm has been outlined and its termination has been established. Further, an upper bound on the number of states of an S-net model has been derived. Since the program uses dynamic memory for storing the state space, a simple coding scheme has been developed to minimize the dynamic memory requirements.

3. Conclusions

S-nets which are equipped with new types of places called signal places and resource places, and scheduler blocks overcome the limitations of DTPNs. S-net model of a multiframe real-time system is intuitively simple whose reachability graph is a semi-Markov chain; standard techniques of stochastic analysis can be used to analyse the underlying system. S-nets are useful for an inegrated analysis of schedulability and performance of hard real-time systems. The performance measures load index and balance index characterize the processor utilization and the uniformity of work load distribution. Computation of specific values for these measures for a real-life example, namely, the computing system onboard a spacecraft demonstrates the need for considering the specific workloads in arriving at a suitable scheduling algorithm. Within this context, S-nets are quite useful tool for the performance evaluation of scheduling algorithms. Automation of state-space generation of an S-net model frees an analyst from the laborious job of constructing the reachability graph. Modelling of sporadic tasks and inclusion of stochastic-timed transitions in S-nets needs further reasearch.

References

1. JORDAN, J. E. Experiences structuring software in a periodic real-time environment, *Software–Practice Experience*, 1990, **20**, 707–718.

2. BALAJI, S., LAWRENCE JENKINS, PATNAIK, L. M. AND GOEL, P. S. — Workload redistribution for fault tolerance in a hard real-time distributed computing system, *Proc 19th Int. Symp. on Fault Tolerant Computing*, Chicago, June 21–23, 1989, pp. 366–373.

3. STOYENKO, A. D., HAMACHER, V. C. AND HOLT, R. C. — Analyzing hard real-time programs for guaranteed schedulability, *IEEE Trans.*, 1991, SE–17, 737–750.

4. CAMPBELL, R. H., HORTON, K. H. AND BELFORD, G. G. — Simulations of a fault tolerant dead-line mechanism, *Proc. 9th Int. Symp. on Fault Tolerant Computing*, Madison, Wisconsin, June 1979, pp. 95–101.

5. DHALL, S. K. AND LIU, C. L. — On a real-time scheduling problem, *Op. Res.*, 1978, 26, 127–140.

6. BALAJI, S., PATNAIK, L. M., LAWRENCE JENKINS AND GOEL, P. S. — S-nets: A Petri net-based model for the performance evaluation of real-time scheduling algorithms, *J. Parallel Distributed Comput.*, 1992, 15, 225–237.

7. ZUBEREK, W. M. — Inhibitor D-timed Petri nets and performance analysis of communication protocols, *IBFOR*, 1986, 24, 231–249.

8. RAMAMRITHAM, K., STANKOVIC, J. A. AND ZHAO, W. — Distributed scheduling of tasks with deadlines and resource requirements, *IEEE Trans.*, 1989, C-38, 1110–1123.

9. ROSS, S. M. — *Stochastic processes*, 1983, Wiley.

Thesis Abstract (Ph. D.)

Performance of multiaccess dual slotted unidirectional bus networks by R. Radhakrishna Pillai
Research supervisor: Utpal Mukherji
Department: Electrical Communication Engineering

1. Introduction

Increased demand for data communication and the advances in optical fibre transmission system technology have made possible the development of high-speed local area networks (LANs) and metropolitan area networks (MANs). Unidirectional bus networks have been proposed for use in the metropolitan area. In such networks, upstream nodes are in a more favoured position for bus access than downstream nodes. Medium access control (MAC) protocols for unidirectional bus networks attempt to alleviate this inherent priority by regulating access to the bus. The distributed queueing MAC protocol[1] of the distributed queue dual bus (DQDB) network attempts to provide fair access on each bus by using a slot request mechanism on the opposite bus. When the ratio d of propagation delay to packet transmission time is large, the distributed queueing protocol preserves throughput fairness through a modification called bandwidth balancing[2]. When the value of d is large, approximate analytical models have been proposed for the distributed queueing protocol[3]. A p_i-persistent access protocol[4] has been proposed in which any node i, if it has a packet to send, accesses an empty slot on the bus with probability p_i, and its performance has been studied for Poisson-offered traffic using approximate analytical models[4,5].

In this work, first, a modified distributed queueing protocol for use in large dual bus networks is proposed and its performance is studied. The protocol has a simpler analytical model compared to the distributed queueing protocol. However, a complete exact delay analysis is found to be difficult. Therefore, the access delay profile of a few quasi-static access schemes is studied in

detail in the case of two nodes accessing a single unidirectional bus. Some of the results required concerning the *Geometric/Geometric*/1 queue are derived. The problem of queue length fairness through dynamic access control in a small network with two nodes accessing a single unidirectional bus is then studied. Finally, the performance of dual bus networks when stations with infinite backlog are connected to the network through low-speed bidirectional channels is studied.

2. A modified distributed queueing protocol for large dual bus networks

Access of one bus, called the data bus, is studied. The other bus is called the request bus. In the modified distributed queueing MAC protocol, a request is moved to the distributed queue at the same time as it is transmitted on the request bus. With this modification, the access delay of a packet at a node is the sum of request bus access delay and data bus access delay. A few properties of the protocol that are independent of the traffic offered to the network are obtained. Some of these properties are used to prove upper bounds on the data bus access delay. To achieve throughput fairness under overload, a rate control similar to the DQDB bandwidth balancing mechanism that retains the traffic-independent properties of the MAC protocol is described, along with the implementation procedure. Thus, under overload, equal throughputs result with bounded data bus access delay. This is useful when the network has to integrate low-volume delay-sensitive traffic with high-volume delay-insensitive traffic. Delay performance of the protocol is studied for Poisson-offered traffic. The request bus access without bandwidth balancing is modelled exactly as a slotted *M*/*D*/1 non-preemptive priority queueing system. Some results for slotted *M*/D/1 queues are obtained and then used to study the performance of request bus access. Expected values of data bus access delay are obtained through simulation. Simulations show that average data bus access delays can be much less than the upper bounds. The expected data bus access delay decreases and the expected request bus access delay increases in the upstream direction. Though this protocol exhibits some desirable properties and permits some exact analysis, a complete exact analysis is not available.

3. Delays in access of a slotted unidirectional bus by two nodes

Some quasi-static schemes for enhancing fairness of bus access delays for two nodes in the absence of feedback from the downstream node are analysed for Bernoulli-offered traffic. The different schemes considered differ in the access control at the upstream node. The downstream node, when its queue is nonempty, accesses an empty slot on the bus with probability 1. The access problem is modelled as a system of two queues with a single shared slotted server.

When access control is absent at the upstream node, the expected delay of a packet at the downstream node is greater than that of a packet at the upstream node. For Bernoulli control, the departure process from the upstream node is Bernoulli and is insensitive to the control parameter value. As a result, the queue lengths at the two nodes at any particular time are statistically independent, and the expected delay of a packet at the downstream node is insensitive to the value of the control parameter. This delay is the same as that in the case without access control. This shows that Bernoulli control is not suitable for Bernoulli inputs. Therefore, two control schemes are considered in which access control at the upstream node is Markovian with two parameters. In the first scheme, access at the upstream node is restricted to only one state of an independent two-state Markov chain. In the other scheme, access probability at the upstream node in any slot is chosen based on the transmission status of the node in the previous slot. In both the schemes, the departure process from the upstream node is a function of the control parameters. In the first scheme, an upper bound on the expected delay at the downstream node is found analytically and in both schemes this expected delay is found through simulation. It is found that there are ranges

of values of the control parameters and packet arrival rates for which the expected delays at both the nodes are less than the expected delay obtained at the downstream node without any access control. It is also found that when the variance of the departure process from the upstream node is less than that of its arrival process, the expected delay at the downstream node is less than that in the case without access control or with Bernoulli control. A method has been devised to solve for the state probabilities of a certain class of multidimensional, irreducible, and positive recurrent Markov chains. The method uses a state variable approach. When the upstream node has infinite number of buffers and the downstream node a finite number, this method can be used to solve the three-dimensional Markov chain arising from a generalized version of the first of the Markovian access schemes.

4. A discrete-time queue with Bernoulli arrivals and state-dependent service rate

A discrete-time queueing system in which the arrival process is Bernoulli and the service rate depends on the number of customers in the system, was considered by Hsu and Burke[6]. The dynamics of the queue were modelled using a three-dimensional Markov chain and Burke's theorem was proved. In this work, a detailed version of the proof is presented. In the special case with state-independent service rate, the queue becomes a *Geometric/Geometric*/1 queue. In that case, the waiting time distribution is obtained. These results, used in the study of access delay performance of the Bernoulli scheme, are mentioned in Section 3.

5. Fairness in queue lengths through dynamic access control

In the special case of bus access by two nodes with negligible propagation delay between them, access of the bus by the two nodes is modelled as a two-queue single server system and the server problem is formulated as a total expected discounted cost minimization problem. The optimal stationary policy in the case of independent arrival processes with arbitrary number of arrivals in a slot and with different arrival rates is obtained with the sum of the squares of the queue lengths as the one-step cost. The optimal policy is work conserving, and it serves the longer queue when the queue lengths are unequal and serves the queue with larger arrival rate when the queue lengths are equal. In the case of 0–1 arrival processes, some sample pathwise results are obtained.

6. Performance of high-speed dual bus networks with input/output bidirectional channel capacity limitation

One of the important applications of a high-speed dual bus MAN is to function as a backbone network interconnecting many low-speed LANs, mainframe computers, and other high-speed devices. Thus, stations may be attached to nodes on a high-speed dual bus network through lower speed local networks or input/output channels. The capacity limitation of the low-speed bidirectional channel that is to be shared for transmission and reception of packets between a station and its node can affect performance. Overload performance is addressed in this work assuming that each station has a very large backlog of packets once it becomes active. Every node is assumed to have one station. Reception at the station is assumed to have priority over transmission from the station through the channel, in order that packet buffering at nodes may be reduced. A communication burst consists of a number of consecutive receptions of packets at a station from its node. The time for which a station has to wait before transmitting depends on the burst length distribution.

In a slotted dual bus network with two stations communicating with each other, in the absence of any control of packet transmission, the steady-state station throughputs and burst lengths de-

pend on the relative activity initiation time and the propagation delay between the nodes. A point of Bernoulli control is introduced between the station and the node, both between the station and the node, and at the node, at the node alone, or at the station. The performance is studied through analysis or simulation, for the case of equal channel and bus capacities. In each of the three schemes that have points of control between the station and the node, both between the station and the node, and at the node, or at the station, the steady-state performance at the two stations is independent of the activity initiation times. The scheme that has points of control both between the station and the node, and at the node, yields the extra flexibility of controlling both throughput and burst length. In the scheme that has point of control between the station and the node, the burst length converges to a geometric distribution when the size of the network is very large. But the channel is not fully utilized in these cases. However, the scheme that has point of control at the node results in different performance of the stations for distinct activity initiation times, but in full channel utilization.

A dual bus network with m, $m \geq 3$, active stations that communicate with one another and with ratio x of channel capacity to bus capacity is also considered. On each network bus, a node has priority in accessing the bus over any node that is downstream of it on the same bus. The steady-state performance depends on the traffic distribution. Traffic distribution is uniform if every station chooses every other station as the packet destination with equal probability, independently for all packets. Conditions for throughput fairness in steady state are obtained for uniform and some non-uniform distributions. As an example, with uniform traffic distribution, the scheme that has point of control between the station and the node results in equal station-to-station throughputs that depend on the value of the control probability p provided that $mx < 4$ or $mx \geq 4$ and $p < 2/(mx - 2)$. However, the channel is not fully utilized when $mx > 4$. With uniform traffic distribution, the scheme that has point of control at the node results in equal throughputs with full channel utilization independent of the control parameter p' provided that $mx < 4$ and $p' > \max_{i,\ 1 \leq i \leq m} \{2(m - i) - x/(4(m - 1) - (2m - i)(i - 1)x)\}$. In a three-node network with $x = 1$, the burst length and node transmit buffer queue length for uniform traffic distribution are obtained through simulation.

References

1. Newman, R. M., Budrikis, Z. L. and Hullet, J. L. — The QPSX MAN, *IEEE Commun.*, 1988, **26**(4), 20–28.
2. Hahne, E. L., Choudhury, A. K. and Maxemchuk, N. F. — DQDB networks with and without bandwidth balancing, *IEEE Trans.*, 1992, **Com-40**, 1192–1204.
3. Tran-Gia, P. and Stock, T. — Approximate performance analysis of the DQDB access protocol, *ITC Specialist Seminar*, Adelaide, 1989, Paper No. 16.1.
4. Mukherjee, B. and Meditch, J. S. — The p_i-persistent protocol for unidirectional broadcast bus networks, *IEEE Trans.*, 1988, **Com-36**, 1277–1286.
5. Mukherjee, B. — An algorithm for the p_i-persistent protocol for high-speed fiber optic networks, *Comput. Commun.*, 1990, **13**, 387–398.
6. Hsu, J. and Burke, P. J. — Behaviour of tandem buffers with geometric input and Markovian output, *IEEE Trans.*, 1976, **Com-24**, 358–361.

Thesis Abstract (Ph. D.)

Stress analysis and strength prediction of pin joints in laminated composite structures by Aruna V. Murthy

Research supervisors: B. Dattaguru, A. K. Rao and B. R. Somashekar(NAL)
Department: Aerospace Engineering

1. Introduction

Fibre-reinforced composite materials have emerged as high-performance materials for a variety of engineering applications. In spite of the many special features composite materials provide, as yet they are not fully exploited for primary structural components, where design against failure becomes very critical. One of the aspects, critical to safe design and performance of a structure is the integrity of all its joints and connections. Large-scale and complex structural systems are fabricated in parts and asembled due to various logistic reasons. The inevitable pin joints in such systems are sources of stress concentration and failure. A safe and efficient design of a structure would necessarily require an understanding of the process of load transfer through these joints. This work is intended to provide an accurate and efficient method of analysis of pin joints in composite structures.

2. Method of analysis

The pin joint configuration is modelled as a circular hole in a laminated composite plate with a circular pin. This two-dimensional system is considered under pin bearing and bypass loads. The basic configuration of pin in the plate could be either interference or clearance or push fit. Under loads pin–plate interface exhibits a state of partial contact/separation above certain load level for all the types of fits. The load–contact variation is nonlinear for misfit pins and is invariant for push fit pins. The major aspect in the solution of the problem of pin joints is the accurate determination of the extent of contact/separation between the pin and the plate. An improved iterative technique is developed based on finite-element method using 8-noded quadrilateral isoparametric elements. A frontal solver combined with a dummy element concept is employed to achieve computational efficiency. The prediction of strength of the joints under bearing (B), shear-out (S) and tensile failure (T) modes is carried out based on maximum stress, average stress and Yamada–Sun failure theories.

3. Numerical studies

The software is validated on several problems of pin joints in isotropic and orthotropic plates for which results are available in literature. Experimental results[1] available in literature are also compiled and for the same configurations, the present method of analysis yielded excellent correlation (often within 10%) (Fig. 1). Studies were carried out on $(0/\pm 45/90)_s$, $(\pm 45)_{2s}$, $(0/90)_{2s}$ and $(0_2/\pm 45)_s$ laminates and typical results shown in figure show that Yamada–Sun criterion provides best correlation to experimental results. Many earlier studies used direct assumption of semicircular arc of contact[2] or cosinusoidal contact pressure[3]. The accurate analysis by the present method indicates that both the assumptions yield inaccurate results in composite plates. Typical plots of normalized radial stress (σ_r/σ_{rmax}) in the region of contact are shown in Fig. 2. It is found that direct assumption could lead to significant errors in the prediction of strength even for orthotropic laminates.

The influence of anisotropy in terms of fibre angle and fibre content in different directions in $(0_m/a_{2n}/90_m)_s$ laminates of T300/5208, (where a is fibre angle and m, n are integers) with pin-loaded

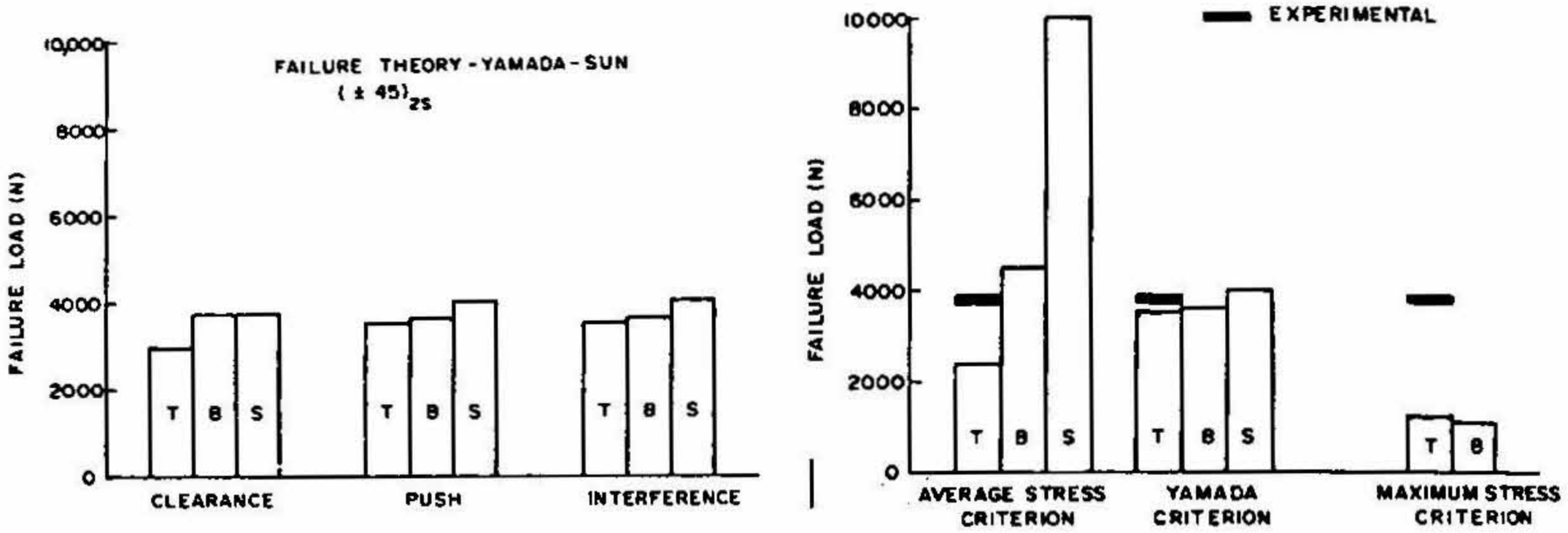

FIG. 1. Failure loads estimated using various failure criteria.

joints, is brought out for the first time. The studies establish that the choice of the laminate is quite critical from the strength point of view and a knowledge of the influence of the laminate paramaters can be effectively used to tailor the joints for specific needs.

Certain layups are found to be weak in certain modes of failure. The numerical results show that $(0/90)_{2s}$ lay up is weak in shear, but strong in tension, whereas $(\pm 45)_{2s}$ layup is stronger in shear but weak in tension.

The concept of a tailored laminate as introduced by Eisenmann[4] is analytically studied. Tailoring the laminate in which the laminate comprises an axial load carrying part with $(0_2/\pm 45)_s$ lay up and bearing load carrying part with $(\pm 45)_{2s}$ lay up, results in improved strength of the joint. For the same configuration, the effect of introducing a metallic/composite bonded bush at the pin hole is examined. An increase of 30% due to tailoring and about 40% due to the presence of a bush is obtained, in the failure load in $(\pm 45)_{2s}$ laminates. However, a cross-ply laminate $(0/90)_{2s}$ shows more sensitivity to the presence of a bush. Studies on the influence of pin elasticity indicate that if the pin stiffness/plate stiffness ≥ 3, it can safely be treated as a rigid pin.

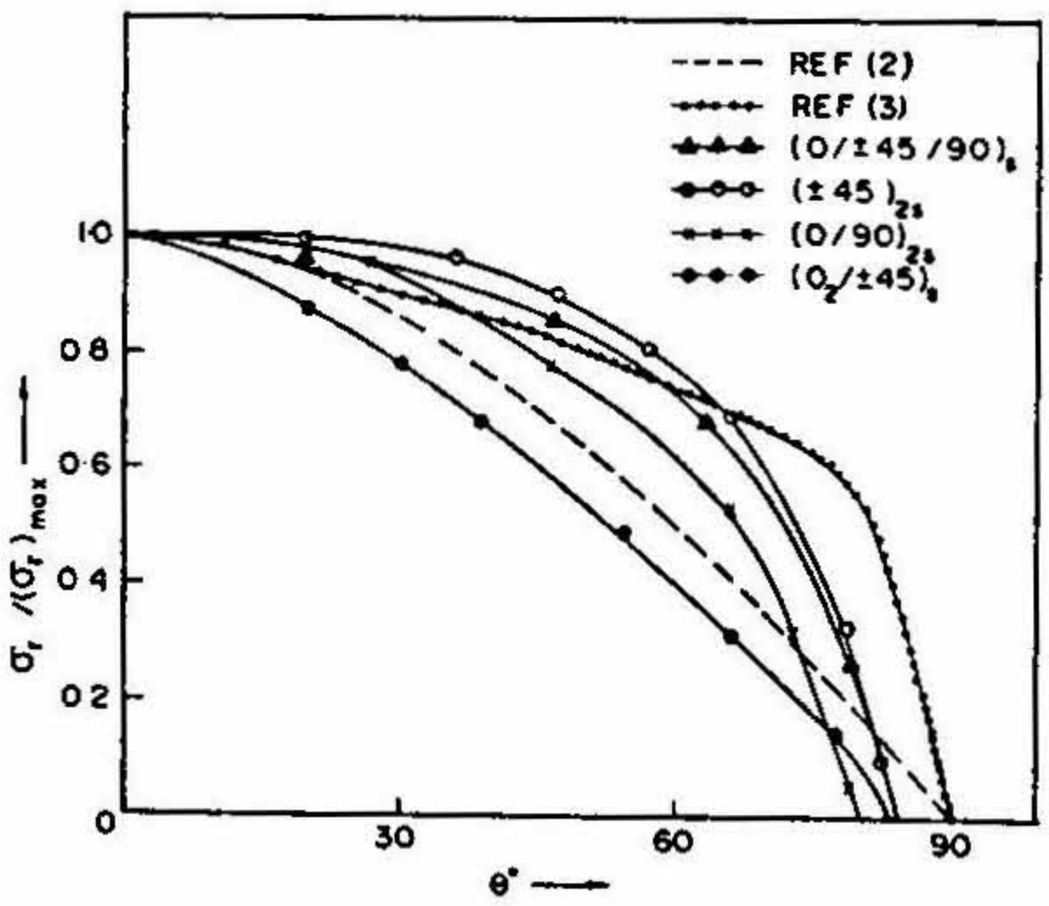

FIG. 2. Normalised radial contact stress for push fit pins.

4. Conclusion

Following conclusions are drawn from this investigation:

1. Simplifying assumptions regarding contact region and contact pressure could lead to significant errors in prediction of strength of pin joints in laminated composites. An accurate method of analysis proposed in the present study, along with Yamada–Sun theory, provides excellent correlation with earlier experimental results (within 10%).

2. The extent of contact/separation and failure characteristics of joints are sensitive to laminate parameters.

3. Two popular design concepts of tailoring and provision of a metallic/composite bush in the laminate are studied to bring out the improved performance of joints.

References

1. VAN SICLEN, R. C. — Evaluation of bolted joints in graphite/epoxy, *Proc. Army Symp. on Solid Mechanics, Role of Mechanics in the design of Structural Joints*, 1974, pp. 120–138.

2. AGARWAL, B. L. — Static strength prediction of bolted joints in composite material, *AIAA J.*, 1980, **18**, 1371–1375.

3. CHANG, F. K., SCOTT, R. A. AND SPRINGER, G. S. — Strength of mechanically fastened composite joints, *J. Compos. Mater.*, 1982, **16**, 470–494.

4. EISENMANN, J. R. AND LEONHARDT, J. L. — *Improving composite bolted joints efficiency by laminate tailoring*, ASTM, STP 749, pp. 117–128, 1981.

Thesis Abstract (Ph. D.)

Helicopter rotor stability in hover and forward flight with a generalized dynamic wake by A. R. Manjunath.

Research supervisors: J. Nagabhushanam and Prasad Sampath (HAL)
Department: Aerospace Engineering

1. Introduction

The importance of lag damping and coupled flap-lag-torsion stability on the design of hingeless rotor blades has been well recognized. The lag damping is crucial to the airworthiness of helicopter, but it is difficult to predict due to the delicate balance of forces in the inplane direction between drag, induced drag and coriolis forces. Moreover, induced drag is sensitive to both trailing and shed components of the unsteady wake.

Research work on the unsteady wake can be attempted through classical aerodynamic, rotor vortex and dynamic inflow theories. The classical unsteady aerodynamic theories are based on frequency domain and their solutions are strictly valid at the stability boundaries and are questionable for damping computation of the system. Vortex theories based on rigid and free wake models are widely used to represent the wake aerodynamics. Limitations from the free wake comes from the fact that one cannot afford to track the unsteady induced flow by numerical integration over hundreds of vortex segments at every time step. In addition, vortex theories, when used in conjunction with blade dynamics, do not lead to desired linearization and conventional

eigenanalysis. In dynamic inflow models, the unsteady effects of wake are introduced into the analysis by consideration of variation of induced flow distribution over the rotor due to unsteady aerodynamic forces. These models can be easily blended with blade dynamics model and directly lead to eigenvalue problem for stability investigations. The Pitt and Peter's 3×3 and 5×5 dynamic inflow models were popularly used in the investigations of flight dynamics[1]. The 3×3 model with three inflow states is the lowest order model to represent wake dynamics with linear radial functions and first harmonic azimuthal inflow distribution. When this model was upgraded to a 5×5 model, the results were not properly interpreted and led to a wrong conclusion that the 5×5 model cannot be used with three-bladed rotor[2]. The reason for the wrong conclusion arose as the number of inflow harmonics required to adequately represent wake dynamics for stability investigations was not properly understood. In recent stability investigations[3] the inadequacy of dynamic inflow to represent the unsteady aerodynamics for high thrust and forward speed has been brought out.

Recently, a powerful generalized dynamic wake model has been developed by Peters *et al.*[4], which includes dynamic inflow (as well as other classical unsteady aerodynamic theories) implicitly. In this theory, the inflow distribution is expanded in an entire set of both harmonic and radial functions, thus representing both higher harmonics and three-dimensional flow effects. The most appealing aspect of this theory is the availability of the expressions for the coefficients of the dynamic wake governing matrices in a closed form. With this type of state-space wake model, it is possible to perform Floquet eigenanalysis with the inclusion of full wake dynamics.

In the present investigation, the dynamic wake model has been utilized to investigate the isolated rotor stability in hover and forward flight. Two interpretive models of isolated rotors are considered. The first model corresponds to rotors with rigid blades having flap-lag motions which is a good representative model for articulated rotors. The second model corresponds to rotors with flexible blades having coupled flap, lag and torsional motions which can simulate the present-day hingeless rotors.

2. Analysis

The rotor blade is treated as a cantilever beam with uniform mass and stiffness properties. The blade is assumed to have no geometric twist and no chordwise offset of the elastic axis or centre of mass. It is assumed to have coupled bending and torsion motions. The structural operators of the blade equations are based on the long, straight, slender, homogeneous isotropic beam with moderate deflections. The aerodynamics is based on linear quasisteady theory and the inflow dynamics is based on the three-dimensional dynamic wake model. The governing equations of motion of the blade are derived by using the variational method based on Hamilton's principle. These equations are coupled with the governing equations of the dynamic wake and solved for trim and stability of the rotor. The total derivation of equations in their explicit form is highly tedious as their expressions are extremely lengthy and unmanageable. In the present investigation, the entire set of governing equations are derived using a special-purpose symbolic processor specially developed for the present investigations. The equations are stored in coded data format and they form input for trim and stability analysis program. In this investigation, the process, starting from the basic steps of derivation of governing equations to final stability analysis, is fully computerized. The results from this approach have been successfully validated by an independent numerical approach demonstrating the reliability of the equations generated through the use of symbolic manipulation techniques.

Several studies are made with the analytical models to find the influence of inflow harmonics on the lag damping estimates, to identify an adequate dynamic wake model leading to reasonably converged damping estimates, to observe the influence of wake dynamics on lag damping estimates at various rotor parameters in comparison with the dynamic inflow model and subsequently to establish the adequacy/inadequacy of dynamic inflow model to represent wake dynamics. Experimental damping data are correlated with the predictions made with dynamic wake model.

3. Conclusions

The following conclusions have been drawn from these investigations:

(1) As the higher inflow harmonics are progressively included in dynamic wake modelling, the predicted lag damping levels show converging but oscillatory trends. These trends are sensitive to advance ratio and to a lesser extent to the number of blades. These oscillatory trends with increasing number of inflow states are almost entirely due to increasing the number of harmonics than due to the number of radial shape functions.

(2) For reasonably good converged damping predictions, at least three radial functions with each harmonic of the inflow are required.

(3) Reasonably converged estimates of all multiblade lag mode dampings can be obtained by considering number of harmonics equal to twice the number of blades.

(4) The influence of the dynamic wake on the lag damping predictions increases with increasing blade loading, lock number and advance ratio.

(5) The damping estimates with dynamic inflow model are away from those with dynamic wake model for all multiblade lag modes thus showing the inadequacy of dynamic inflow model for stability investigations. This inadequacy increases with increase in blade loading, lock number and advance ratio.

(6) The lag dampings are sensitive to wake dynamics both for soft and stiff inplane rotors. In general, the influence of wake dynamics is more significant for stiff inplane rotors as compared to soft inplane rotors.

(7) For a flexible bladed rotor with low torsional blade frequency, it is observed that at least nine inflow harmonics are needed.

(8) Two uncoupled modes each for flap, lag and torsion motions can give good converged first lag damping estimates.

(9) In hover, the wake dynamics has a stabilizing effect on the first lag mode at high torsional frequencies and this effect seems to reduce fast as low torsional frequencies are approached. However, at high advance ratio, this stabilizing effect seems to increase with decrease to torsional frequencies.

(10) Wake dynamics has strong influence on both the first and second flap mode dampings at all advance ratios and their influence is to decrease the dampings of the flap modes. The wake dynamics seems to influence second flap-mode dampings more compared to the first flap-mode dampings.

(11) Wake dynamics has varied influence on the first torsion-mode dampings with advance ratio, torsional frequency and they are different with each of its multiblade modes. In general, the observed influence is to increase the dampings of all its multiblade modes. The second torsion-mode dampings are not influenced by the wake dynamics.

(12) The predicted lag regressive mode dampings with both idealizations of rotors with rigid and flexible blades of a model rotor are correlated with test data. These studies show that the dynamic wake model consistently improves correlation better than dynamic inflow model both in hover and forward flight.

(13) Symbolic manipulation techniques can be effectively utilized even when the system state variables are greater than 100.

References

1. PITT, D. M. AND PETERS, D. A. Theoretical prediction of dynamic inflow derivatives. *Sixth European Rotorcraft and Powered Lift Aircraft Forum*, Bristol, England, September 1980.

2. NAGABHUSHANAM, J. *Rotorcraft air resonance in forward flight with various dynamic inflow models and aeroelastic couplings*, Ph.D. Thesis, Indian Institute of Science, Bangalore, India, 1984.

3. TOROK, M. S. AND CHOPRA, I. Hingeless rotor aeroelastic stability analysis with refined aerodynamic modeling, *Am. Helicop. Soc.*, 1991, 36, 48–56.

4. PETERS, D. A. AND HE, C. A closed form unsteady aerodynamic theory for lifting rotor in hover and forward flight, *Proc. 43rd Annual National Forum of the American Helicopter Society*, St. Louis, Missouri, May 1987.

Thesis Abstract (M.Sc. (Engng))

Damage and its growth in laminated composite circular plates undergoing large deformations by Chitturu Sridhar

Research supervisor: K. P. Rao

Department: Aerospace Engineering

1. Introduction

Composite materials such as carbon fibre-reinforced plastics are finding increased use in a wide range of both low- and high-technology engineering applications. However, they suffer some serious limitations. The most significant among these is their response to low-velocity impacts such as that imparted by a dropped tool or runway debris. Tests by previous researchers have shown that the composite laminates undergo large displacements under impact. Hence for an accurate prediction of damage in thin laminated composites due to low-velocity impacts, incorporation of geometric nonlinearity is necessary. The nonlinear analysis and damage estimation of composite laminates is a complex problem. Furthermore, low-velocity impact problem can be treated as a quasi-static problem, because the impact duration is much longer than the time required by the propagating waves to travel from the impact site to the supports.

The present study is aimed at the formulation of geometric nonlinear finite-element analysis and using it in the estimation of damage and its growth in laminated composite circular plates. Damage modes are limited to ply splits and fibre breaks.

2. Nonlinear finite-element analysis

A 4-noded 48 d.o.f doubly curved quadrilateral laminated anisotropic shell finite element was developed by Venkatesh and Rao[1]. The element is bound by two parallel circles and two meridians of a shell of revolution. Each node has 12 degrees of freedom. The various d.o.f are

$$\{q\}=\left\{u,\frac{\partial u}{\partial s},\frac{\partial u}{r\partial\theta},\frac{\partial^2 u}{r\partial s\partial\theta},\ v,\frac{\partial v}{\partial s},\frac{\partial v}{r\partial\theta},\frac{\partial^2 v}{r\partial s\partial\theta},\ w,\frac{\partial w}{\partial s},\frac{\partial w}{r\partial\theta},\frac{\partial^2 w}{r\partial s\partial\theta}\right\}.$$

First-order Hermite interpolation polynomials are used to describe the three displacements u, v and w. Presently, this element is particularised for obtaining a sector element and is used to solve the large deformation problem of laminated composite circular plates.

The linear elastic and tangent stiffness matrices $[K_I]$ and $[K_T]$ are obtained following the conventional procedures. Finally to get the nonlinear deflections Newton–Raphson method is used as a nonlinear solution technique.

3. Estimation of damage

The contact between the impactor and the plate is assumed to obey the Hertzian law. Stresses are computed using nonlinear finite-element analysis at every Gaussian point in all plies. Subsequently, at all the Gaussian points of all plies, a check is made for failure using Tsai–Wu criterion. If failure is detected at a point, the material properties of the ply at that point are degraded. The geometric nonlinear analysis is again carried out after having accounted for damage and the new stresses are obtained. The process is continued iteratively till no further damage is detected.

4. Results and discussion

A computer code is developed using the method proposed and checked for correctness by solving examples of isotropic and orthotropic circular plates for which solutions are available in literature. Next, the case of a T300/N5208, [45°/0°/–45°/90°]-laminated circular plate impacted by a spherical impactor is considered. Figure 1 shows the load-displacement relationship for the plate obtained by the present analysis as well as the results of Elber[2] and Shivkumar *et al.*[3] Good agreement is seen. Figure 2 shows the overall size of the damage (superimposed view of all ply damages) in the late for each load value. The damage plots are similar to what can be observed in an ultrasonic-C scan of the damaged plate. Figure 3 shows the damage in the individual plies for a load of 0.5 kN.

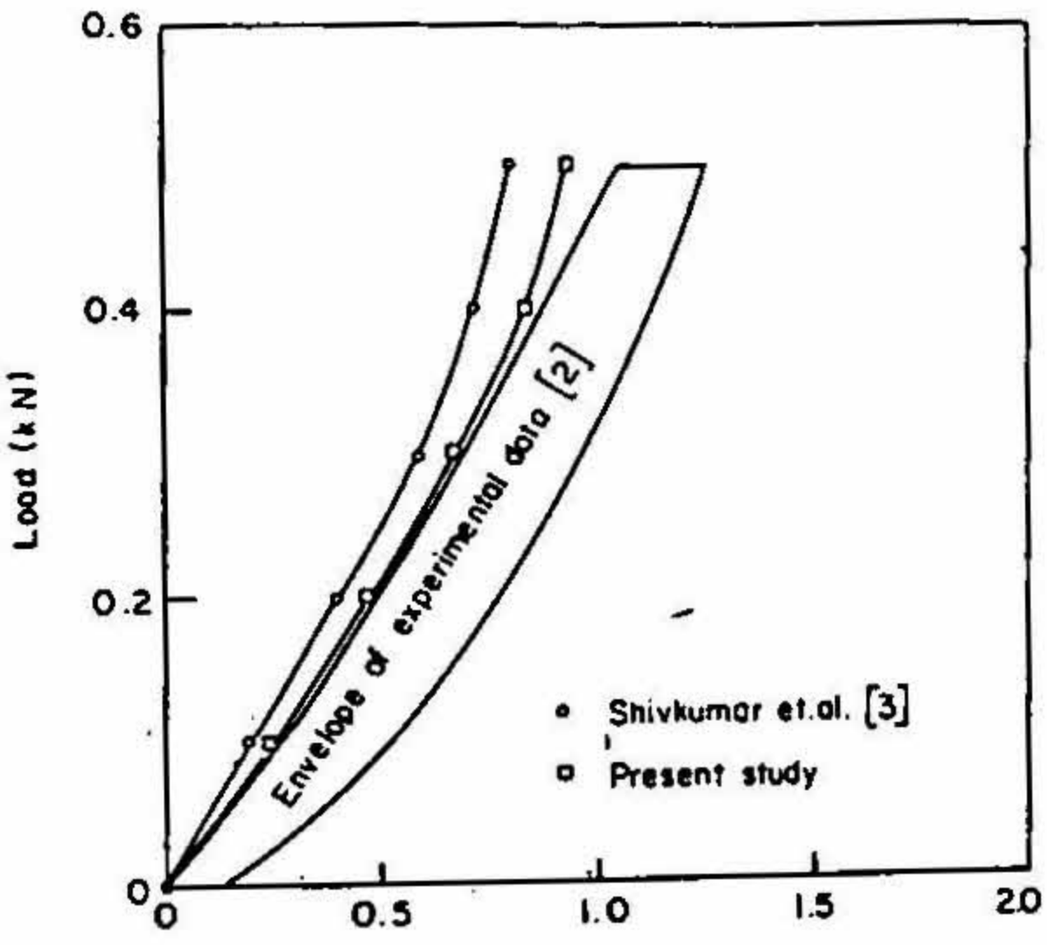

FIG. 1. Comparison of results of Elber[2] and Shivakumar *et al.*[3] with the present study.

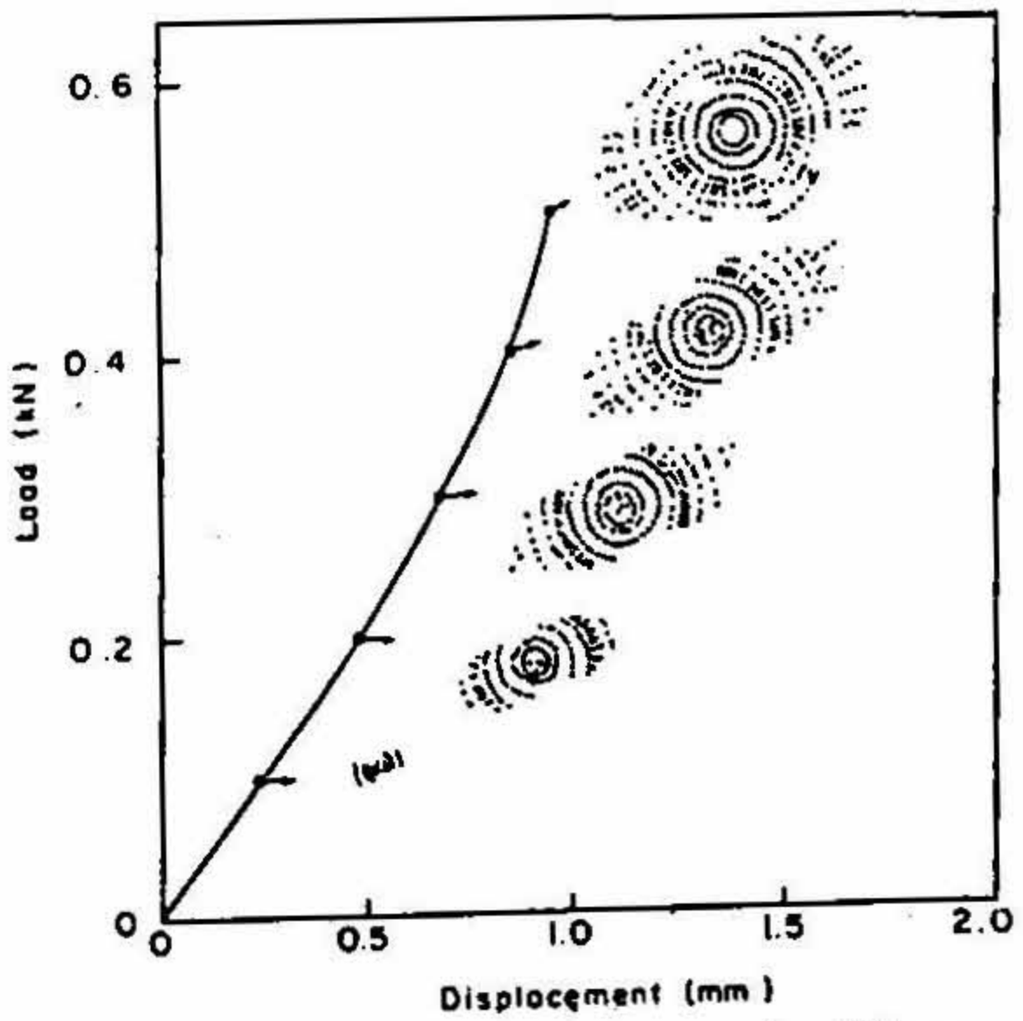

FIG. 2. Superimposed damage patterns for different load values.

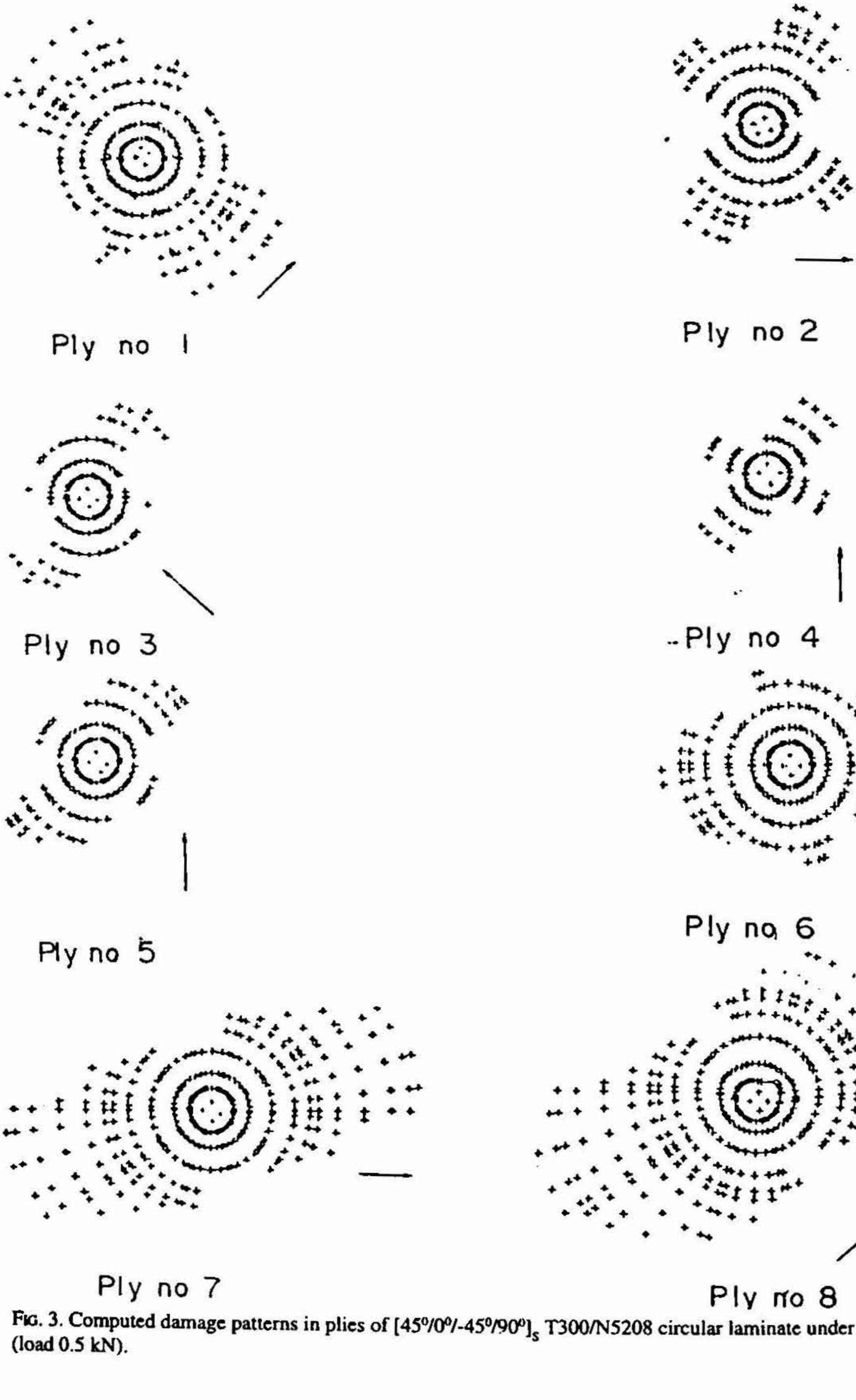

FIG. 3. Computed damage patterns in plies of $[45^0/0^0/-45^0/90^0]_s$ T300/N5208 circular laminate under impact (load 0.5 kN).

5. Conclusion

A nonlinear finite-element analysis has been made using a 48 d.o.f. sector element for the estimation of damage in laminated circular composite plates due to low-velocity impact. The low-velocity impact problem is treated as an equivalent large deformation quasi-static problem. The Hertzian contact is assumed. Tsai–Wu criterion is used to find the zones of failure. The constitutive law is suitably degraded in the failed zones and used in the subsequent iterations. The problem of a T300/N5208, $[45°/0°/-45°/90°]_s$ circular-laminated plate being impacted by a spherical impactor is solved. The method developed can easily be extended to study the low-velocity impact damage in composite rectangular plates and axisymmetric shells/shell panels.

References

1. VENKATESH, A. AND RAO, K. P. — A doubly curved quadrilateral finite element for the analysis of laminated anisotropic thin shells of revolution, *Comput. Struct.*, 1980, 12, 825–832.
2. ELBER, W. — *Failure mechanics in low-velocity impacts on thin composite plates*, NASA Technical Paper 2152, May 1983.
3. SHIVKUMAR, K. N., ELBER, W. AND ILLG, W. — Prediction of low-velocity impact damage in thin circular laminates, *AIAA J.*, 1985, 23, 442–449.

Thesis Abstract (M.Sc. (Engng))

A new parameterization of atmospheric heating for simple models of relevance to ENSO by N. H. Saji

Research supervisor: B. N. Goswami

Department: Centre for Atmospheric Sciences

1. Introduction

The El Nino Southern Oscillation (ENSO) phenomenon, which is one of the prominent signals of interannual variability in the tropical ocean–atmosphere system, has attracted the attention of researchers world wide. This is due to its effect on climate locally as well as globally and due to its potential to affect life in general through such climate anomalies. Experiments with numerical models of the coupled ocean–atmosphere system have thrown light on many aspects of ENSO, yet many more aspects remain unclear. It has been appreciated that a better understanding of ENSO is crucially dependent on the improvement of the present coupled models which exhibit serious systematic errors like climate drifts. In the present work, we take a step in that direction by developing an improved atmospheric model which can be used as the atmospheric component in a simple or a hybrid coupled model. This model as we show has overcome many of the drawbacks that have been noticed in the existing simple atmospheric models.

2. Problems with simple atmospheric models

Two of the doubtful aspects of simple models are the assumption of linear dynamics and the way in which atmospheric forcing has been parameterized in terms of sea-surface temperature anomalies (SSTA). Most simple models employ Gill-type linear dynamics[1] and the atmospheric forcing is assumed to arise from the latent heat release associated with large-scale organized convection. Many studies have suggested that the assumption of linear dynamics is indeed a valid one and

that realistic simulation of surface winds is possible with a linear model if the atmospheric heating is prescribed correctly[2,3].

We have looked critically into the way in which large-scale organized deep convection has been parameterized in simple models. Many of these models assume that anomalies in deep convection are more or less linearly dependent on SSTAs. As a consequence the forcing in such models has the structure of the underlying SSTAs. A comparison of the anomalies of deep convection, parameterized in this manner, with outgoing longwave radiation (OLR) anomalies (*OLR anomalies have proved to be a good proxy for anomalies in deep convection in the tropics*) show that the parameterized heating field differs significantly from the observed field. Another interesting study, in which information about surface winds was fed into a simple linear atmospheric model to infer the forcing field, revealed that the inferred forcing differed significantly from the corresponding SSTA field but resembled the OLR anomaly field rather closely[3].

We are strongly critical of the assumption of the linear relationship between SSTAs and deep convection anomalies. Our objection is based on the increasing amount of observational[4,5] and theoretical evidence for the existence of an SST threshold of 28° C for the onset of deep convection. The implication of this threshold is that when the SST is below the threshold an SSTA would have no effect on deep convection since no deep convection existed in the first place. On the other hand, an SSTA would modulate the deep convection above waters which had SST equal to or greater than the threshold.

3. A new parameterization of deep convection

We have proposed a new parameterization of deep convection, the novel feature of it being the explicit inclusion of an SST threshold of 28° C for deep convection. We find that the inclusion of the SST criterion has improved the representation of deep convection quite significantly. The

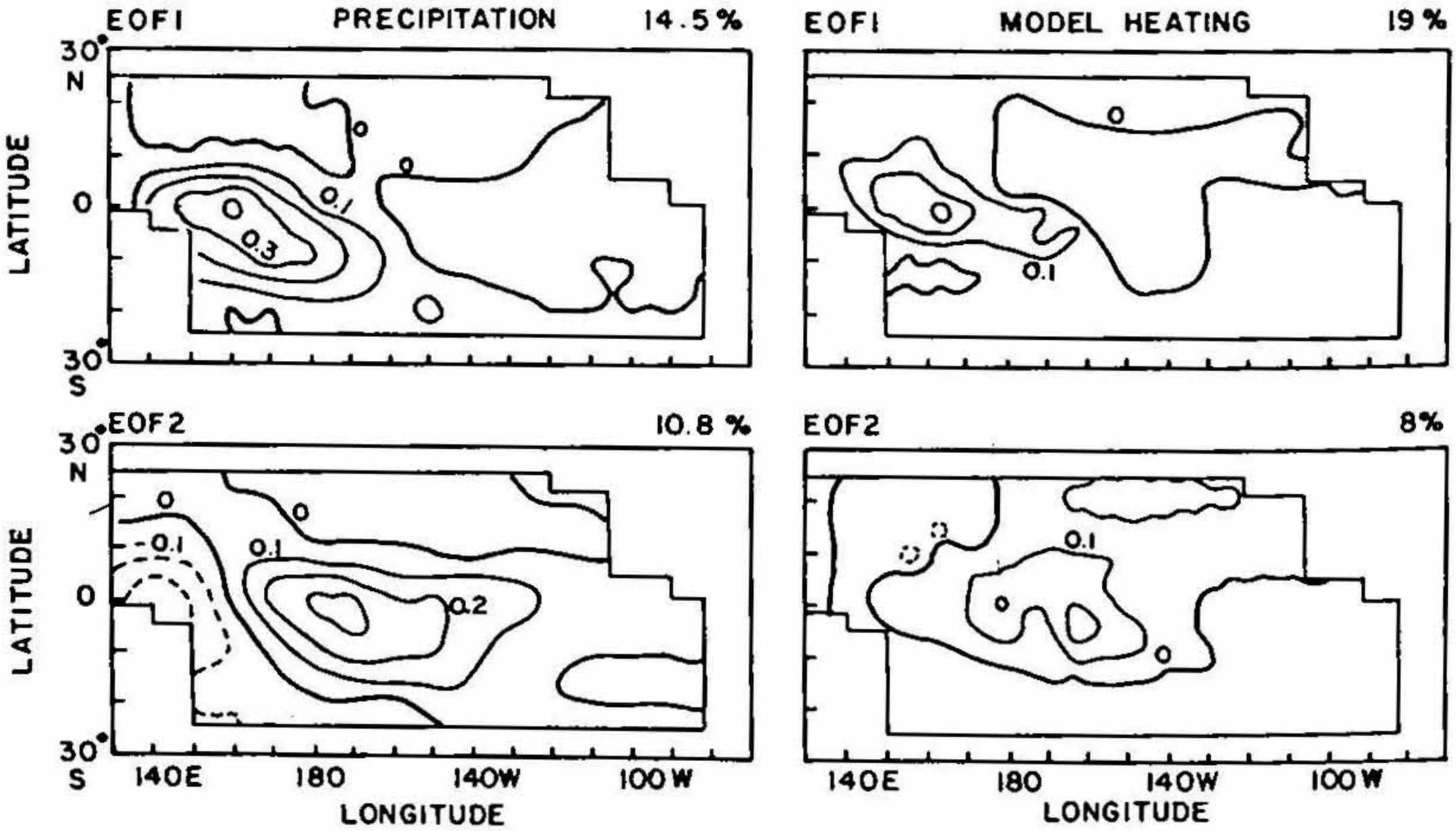

FIG. 1. The first two EOFs of the precipitation anomaly compared with those of the heating anomaly given by the new parameterization. Zero contour is bold, negative contours are dashed.

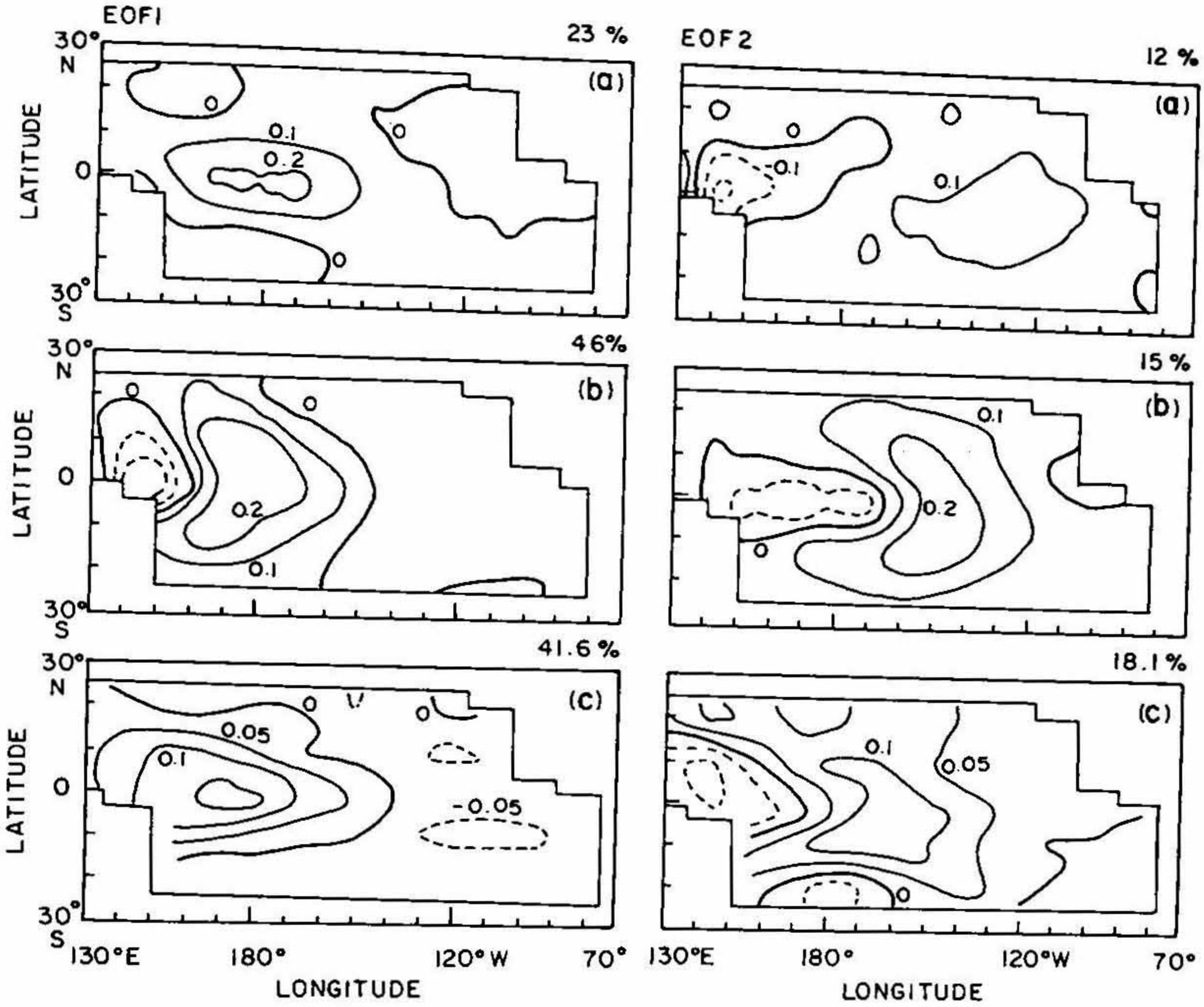

FIG. 2. EOF1 and EOF2 of zonal wind anomalies obtained from a. observations (COADS winds), b. the linear model, and c. the ECMWF T-21 AGCM. Zero contour is bold, negative contours are dashed.

parameterized forcing field is now very different from the SST anomaly field and bears quite remarkable resemblance to the outgoing longwave radiation (OLR) anomaly field. We also conducted a comparitive study of the variability in the model forcing field with that in the observed OLR anomaly field. The empirical orthogonal function analysis (EOF) was employed for this purpose. This analysis showed that the new parameterization is able to capture well the large-scale features of the variability in the observations (Fig. 1).

4. The atmospheric model simulations

Our atmospheric model employs simple Gill-type linear dynamics and is, in this way, similar to the existing simple models of the tropical atmosphere. The only difference is in the new parameterization of deep convection that we have proposed. The model was integrated with the parameterized heating field for each of the 168 months from Jan 1974 to Dec 1987. The model-simulated surface winds were found to bear good resemblance to the observed winds. We also find that the problem of spurious easterlies has been reduced considerably in strength and north-south extent. An EOF analysis on the observed and simulated surface wind anomalies showed that our model

with the new parameterization was able to simulate the large-scale part of the observed variability quite well. In fact, it was found to closely resemble, in this respect, results from a similar analysis on a complex atmospheric general circulation model (Fig. 2). We believe that this is an important accomplishment because investigations[6,7] have revealed that it is the large-scale features of the surface wind variability that are important for the interannual variability in the oceans.

References

1. GILL, A. E. *Q. J. R. Met. Soc.*, 1980, **106**, 447–462.
2. NEELIN, J. D. *Q. J. R. Met. Soc.*, 1988, **114**, 747–770.
3. ZEBIAK, S. E. J. *Climate*, 1990, **3**, 1016–1031.
4. GADGIL, S., JOSEPH, P. V. AND JOSH, N. V. *Nature*, 1984, **312**, 141–143.
5. GRAHAM, N. E. AND BARNETT, T. P. *Science*, 1987, **238**, 657–659.
6. LATIF, M. *et al.* *J. Climate*, 1990, **3**, 509–521.
7. GOSWAMI, B. N. AND SHUKLA, J. *J. Climate.*, 1991, **4**, 3–22.

Thesis Abstract (M.Sc. (Engng))

Development of an optimal iterative method for optical tomographic reconstruction of highly varying refractive index distributions by J. R. Suman Nirmal

Research supervisors: R. M. Vasu and G. V. Anand
Department: Instrumentation and Services Unit and Electrical Communication Engineering

1. Introduction

Optical tomography is a special case of the well-known X-ray computer-assisted tomography. In X-ray tomography we measure the total attenuation of the X-ray passing through the object (such as tissues of biological specimens) and reconstruct cross-sections of the object. In optical tomography we illuminate the object (usually refractive index distributions) with coherent light and measure the total time of flight (or phase delay) of the light traversing through the object. In objects that have highly varying refractive index distributions the light rays travel along curves instead of straight line paths that the X-rays take. Hence the analytical and iterative methods that are available to solve the X-ray tomographic problem cannot straightaway handle the optical tomographic inversion. This work develops an optimal iterative method for inverting phase delay data of optical tomography.

2. Methodology

In X-ray tomography there are two approaches to the solution: (*i*) the analytic, and (*ii*) the iterative approach. All analytic methods can be traced back to one important theorem of tomography called 'central slice theorem'[2]. The iterative methods are based on 'series expansion' and modelling the forward X-ray transmission through the object as matrix-vector equations of the type $Ax = b$. The algebraic reconstruction technique (ART) is one such very successful iterative method[4].

It has been observed that there are no straightforward analytic formulae available for optical tomographic inversion, nor is it possible to incorporate refraction error into the existing analytic reconstruction formulae of X-ray tomography. But the iterative methods are flexible enough to

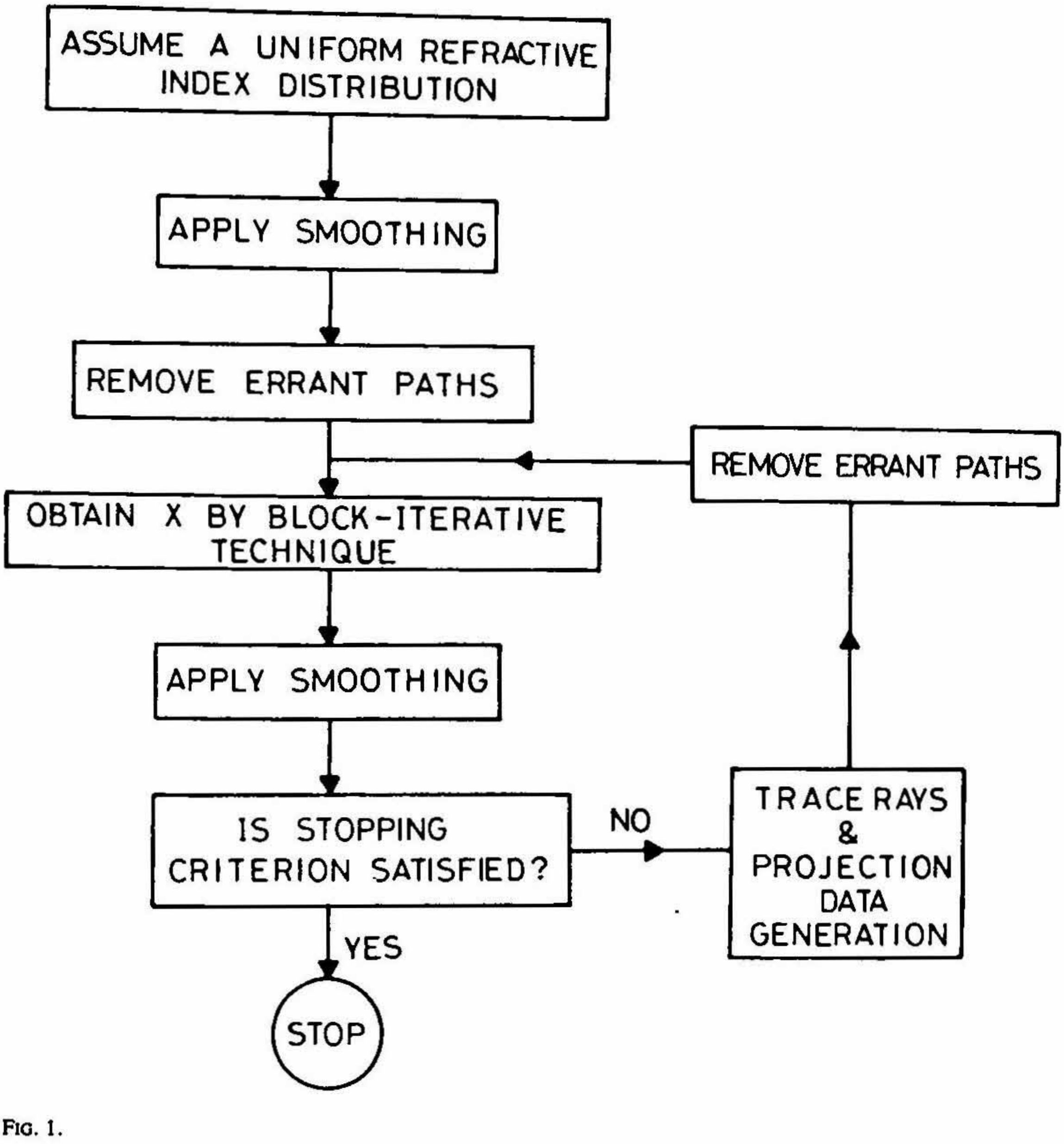

FIG. 1.

incorporate corrections for ray bending[5]. Lira and Vest[6] devised two such modifications known as straight line inversion with modified data (SLIM) and the curved ray algebraic reconstruction (CRAI). We have developed here an iterative procedure (Fig. 1) which is similar to CRAI. This procedure contains two important steps, namely, the forward propagation of light through the object carried out with the help of an efficient ray-tracing algorithm and the inversion of these data through an ART-type inversion procedure. The other steps are the incorporation of known constraints both in the object and the projection space. We have used both block-iterative additive ART and multiplicative ART (MART) for inversion[3]. The other factors we kept in mind were: (*i*) the rays which deviated by more than 0.5 radians were eliminated[1], (*ii*) the relaxation parameter was optimized both for MART and additive ART, (*iii*) the object estimate after each

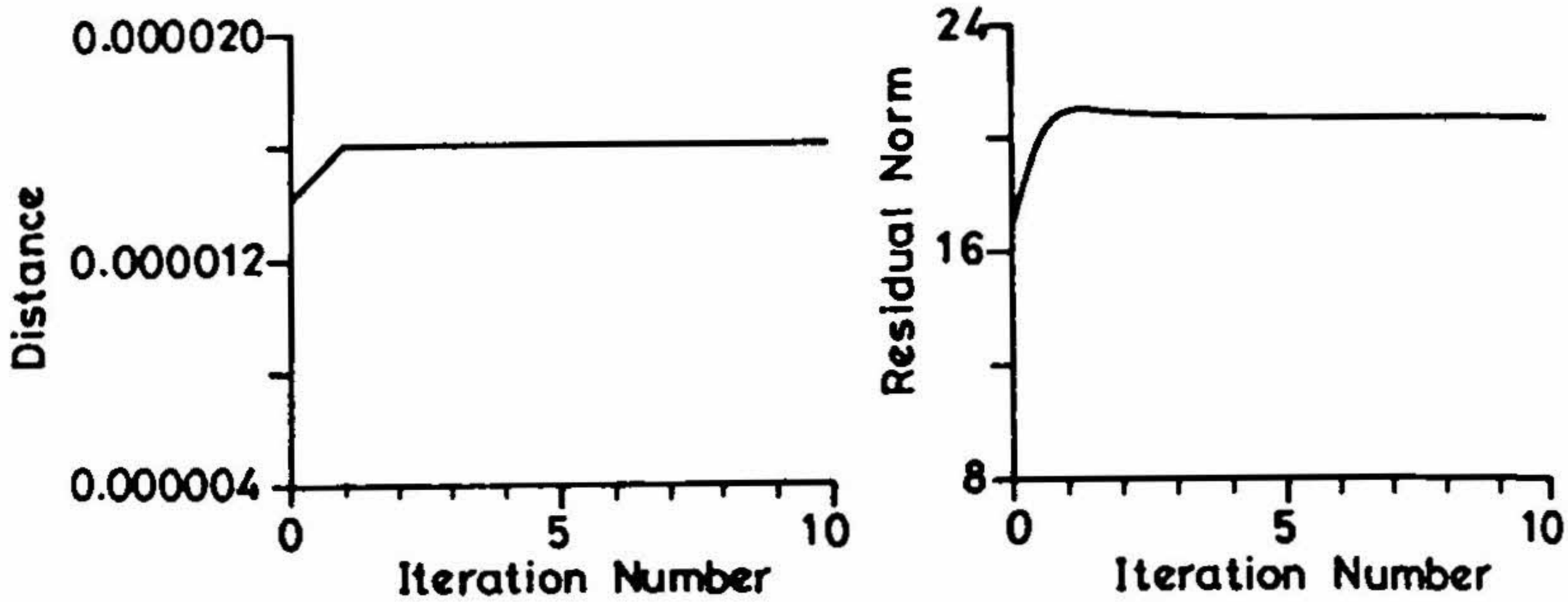

FIG. 2. Block iterative ART without ray-tracing on test image 1.

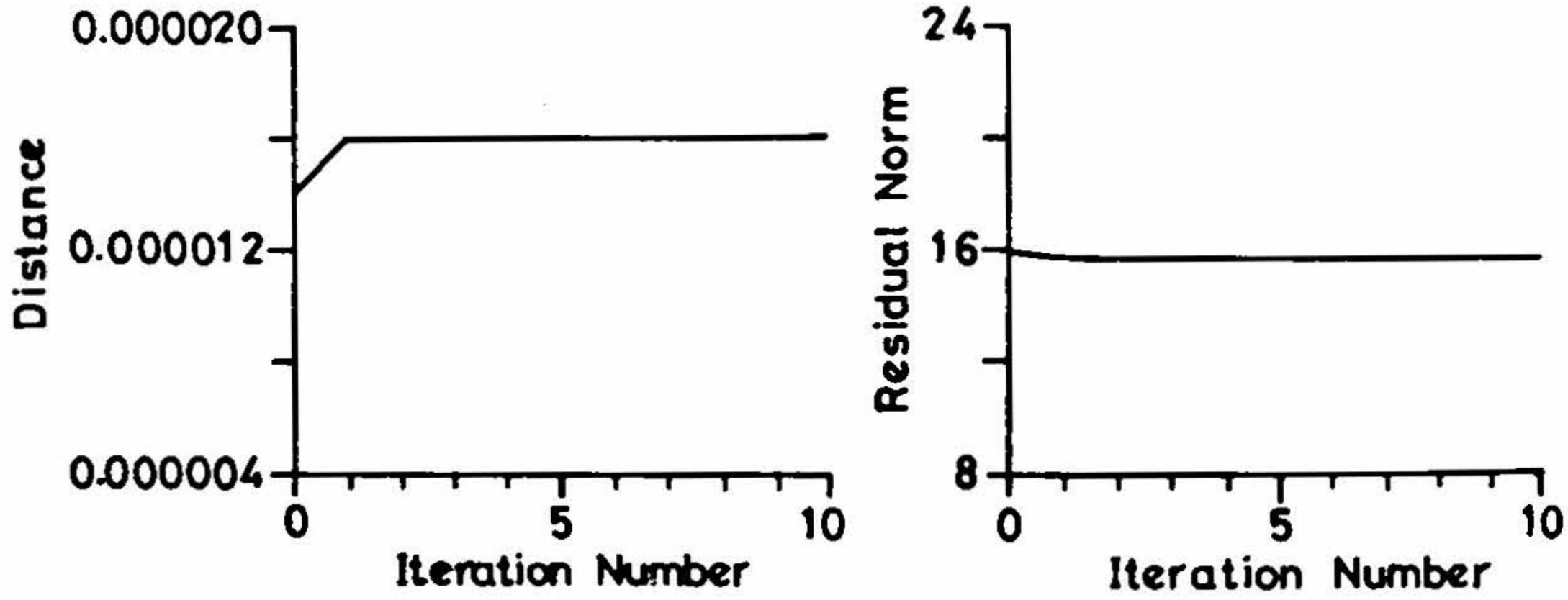

FIG. 3. Block iterative ART without ray-tracing on test image 2.

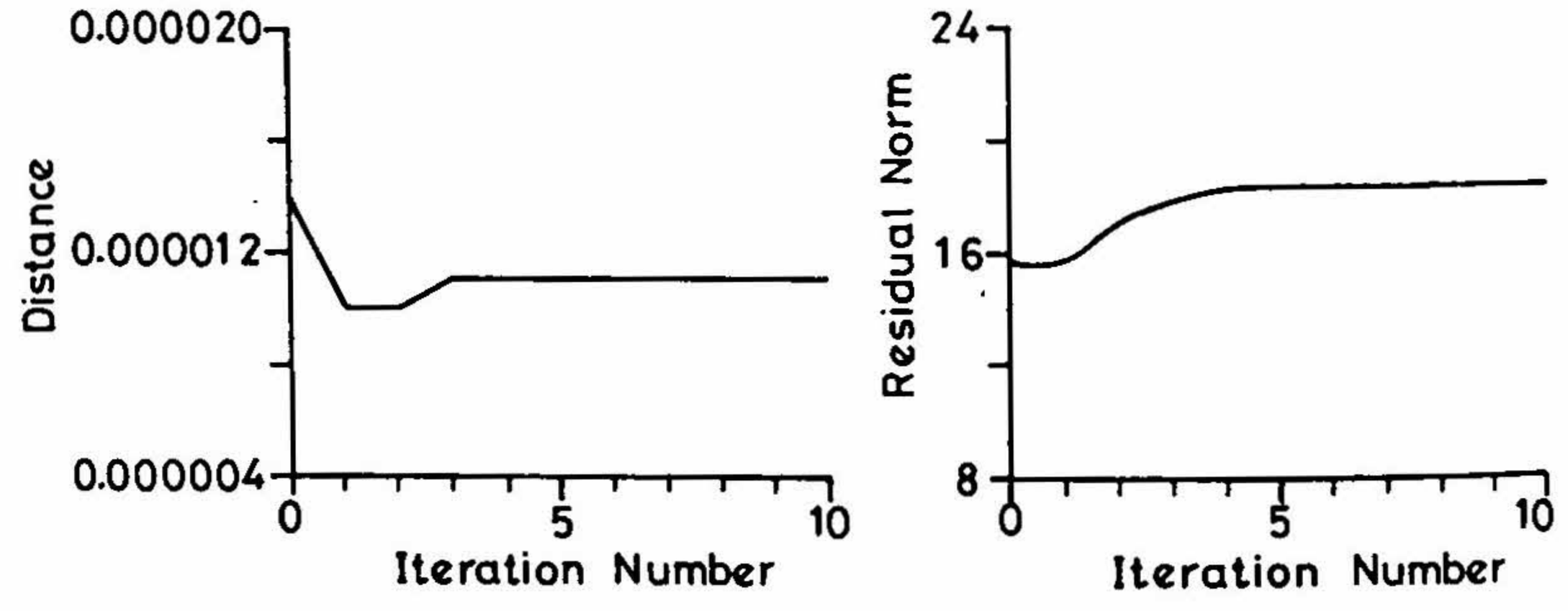

FIG. 4. Block iterative MART without ray-tracing on test image 1.

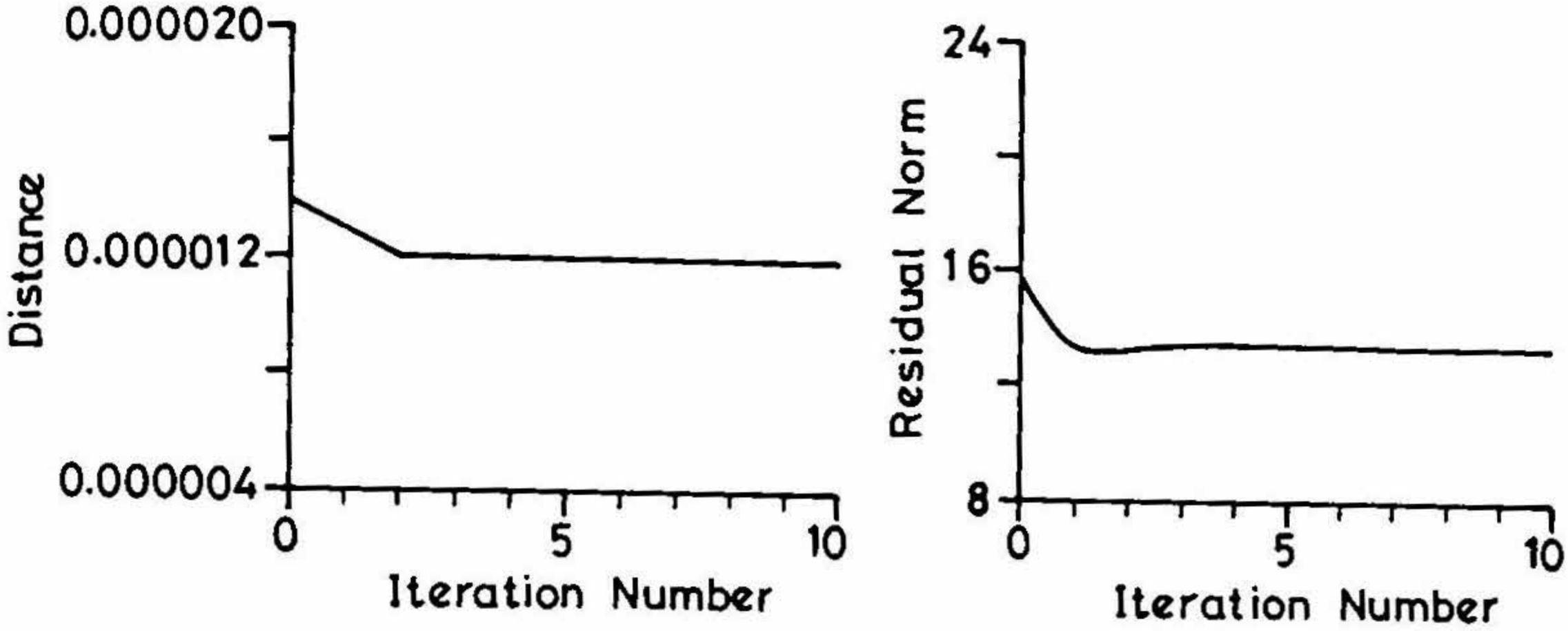

FIG. 5. Block iterative MART without ray-tracing on test image 2.

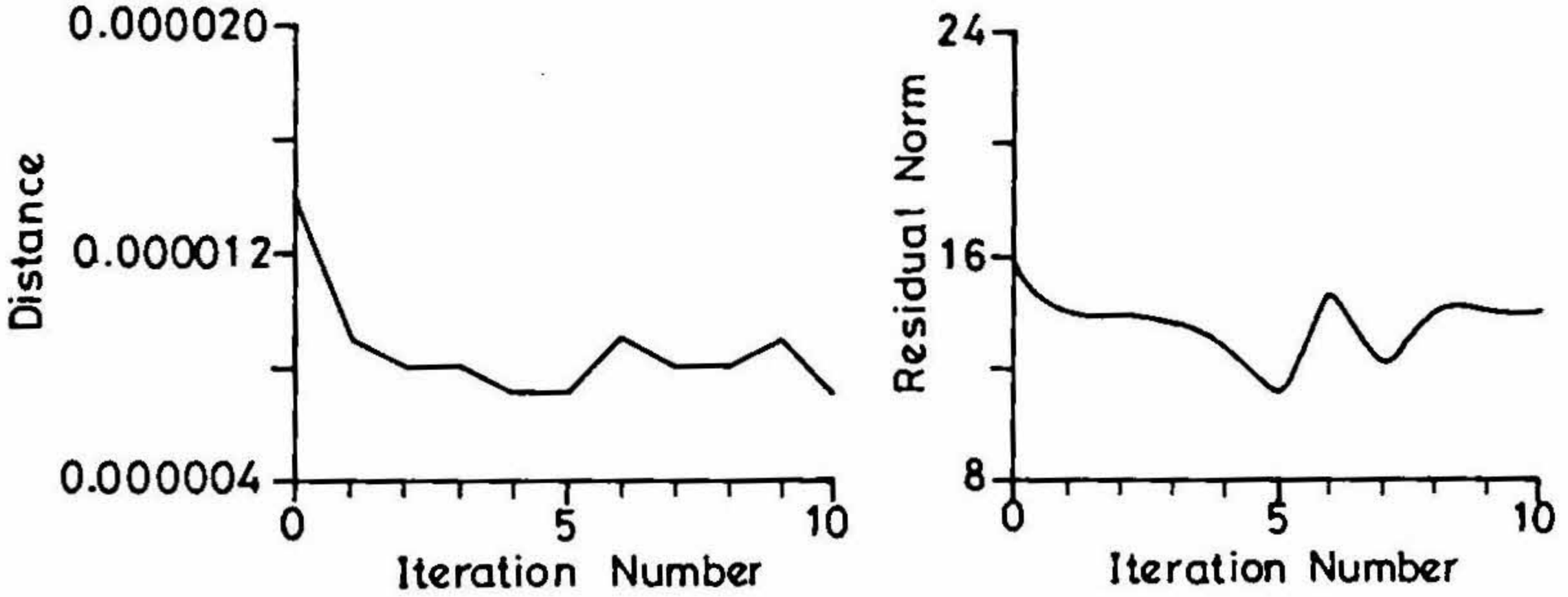

FIG. 6. Block iterative ART with ray-tracing on test image 1.

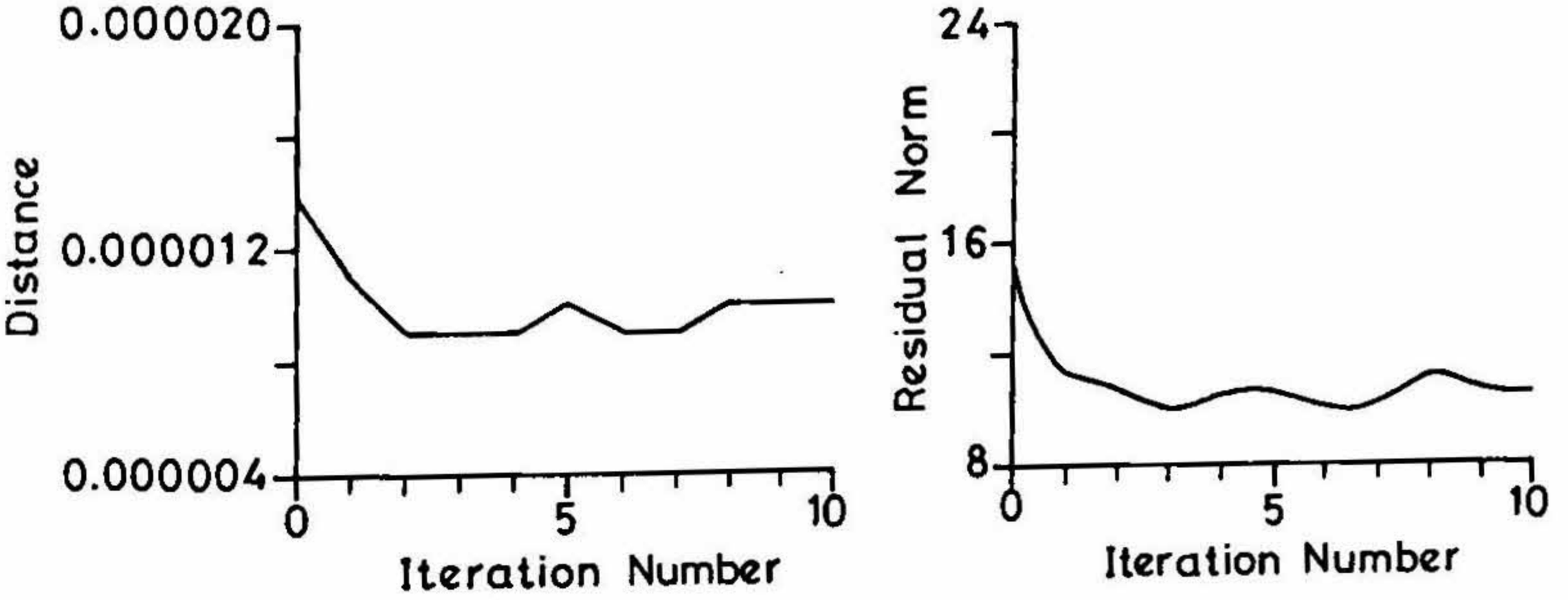

FIG. 7. Block iterative ART with ray-tracing on test image 2.

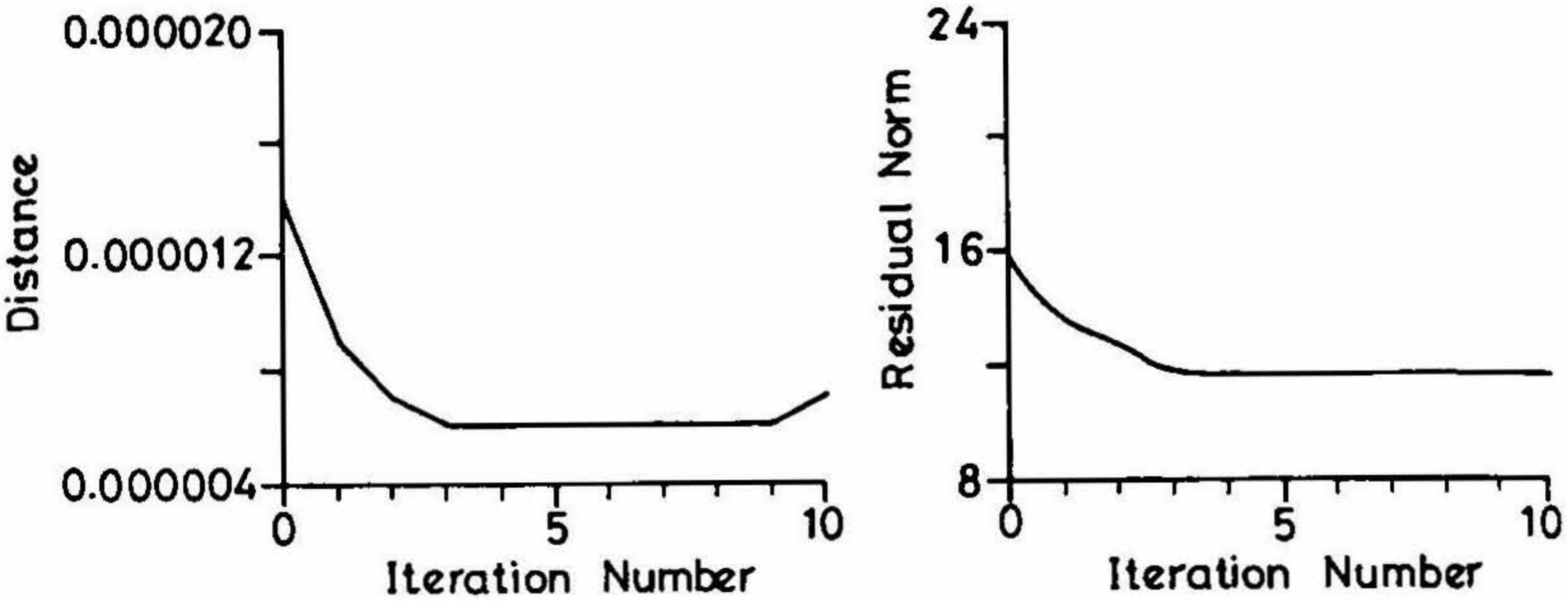

FIG. 8. Block iterative MART with ray-tracing on test image 1.

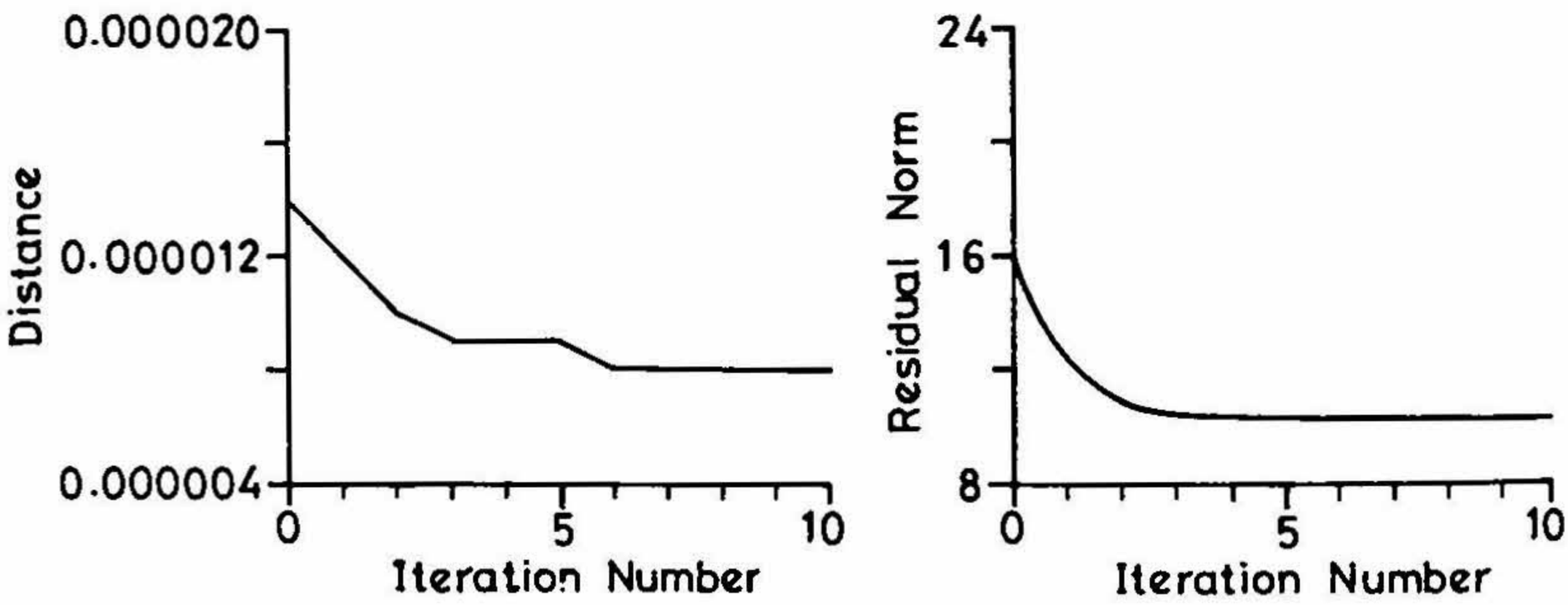

FIG. 9. Block iterative MART with ray-tracing on test image 2.

iteration was selectively smoothed, and (*iv*) the a priori knowledge of the upper and the lower bounds of the object were incorporated in the object estimate. These steps ensured that the iteration converged quickly giving reasonably good estimates of the object. To estimate the quality of reconstruction, distance measures in both the object and projection space were used. Numerical experiments were done over two simulated objects, namely, the Shepp–Logan Head phantom (test object 1)[4] and the Spikes phantom (test object 2)[7]. The experiments were repeated under the following conditions:

(i) block iterative ART for inversion and forward propagation along straight lines.

(ii) block iterative MART for inversion and forward propagation along straight lines.

(iii) block iterative ART for inversion and forward propagation through ray tracing.

(iv) block iterative MART for inversion and forward propagation through ray tracing.

Figures 2–9 show how the error estimates vary with iteration number

3. Results and conclusion

It is seen clearly that when block-iterative methods were used without ray tracing the error estimates either increased or decreased only by a small amount. This is due to the erroneous modelling of the propagation of light beam through the object by straight-path approximation. When ray tracing was incorporated, the error estimates decreased. The redistribution of error (during the iteration) amongst the pixels is more accurate in the case of block-iterative MART as compared to block-iterative ART. We thus conclude that an iterative procedure incorporating ray-tracing and the block-iterative MART is the most appropriate to reconstruct highly varying refractive index distributions. The local smoothing, tuning the relaxation parameter and the elimination of rays that deviate by more than the pre-set tolerance angle are all applied to arrive at a good reconstruction.

References

1. BERRYMAN, J. G. — Fermat's principle and nonlinear traveltime tomography, *Phys. Rev. Lett.*, 1989, **62**, 2953–2956.
2. DEANS, R. L. — *Radon transform and some of its applications*, 1983, Wiley.
3. HERMAN, G. T. AND LEVKOWITZ, H. — Initial performance of block-iterative reconstruction algorithms, *Mathematics and computer science in medical imaging*, 1987, NATO ASI Series, Vol. 39, pp. 305–307.
4. HERMAN, G. T. — *Image reconstruction from projections. The fundamentals of computerised tomography*, 1980, Academic Press.
5. HESSELINK, L. — Optical tomography. In *Handbook of flow visualization* (W. Yang, ed.), 1989, pp. 307–329, Hemisphere Publishing.
6. LIRA, I. H. AND VEST, C. M. — Refraction correction in holographic interferometry and tomography of transparent objects, *Appl. Opt.*, 1987, **26**, 3919–3928.
7. VERHOEVEN, D. D. — *Application of computed tomography and holographic interferometry to the study of transparent media*, Tech. Rep. 38501, Institut Francais du Petrole, Ruil-Malmaison, France, 1990.

Thesis Abstract (Ph. D.)

Development of a jet with local buoyancy enhancement by R. Elavarasan

Research supervisors: M. A. Ramaswamy, A. Prabhu and G. S. Bhat

Department: Aerospace Engineering

1. Introduction

There are many practical as well as neutral flows in which buoyancy enhancement takes place, for example, due to chemical reaction (combustion), phase change (flows in cumulus), etc. These kind of flows have not been studied well. The present work attempts to understand a flow with increasing buoyancy, in particular, an axisymmetric (round) jet subjected to volumetric heating.

In the previous studies[1,2] techniques had been used for producing buoyancy enhancement where mixing is a prerequisite for the production of buoyancy. So effect of buoyancy enhancement on mixing could not be clearly separated. In the present experiment, an ohmic heating technique[3] has been used thus avoiding any chemical reaction.

HR - heated region
CT - constant temp bath
FL - focussing lens
TR - traverse
T - tank
N - nozzle
PS - particle seeder
A,B,C - control valve
R - reservoir
M - manometer
G - grids
BF - brass frames
WL - water level
S - screen

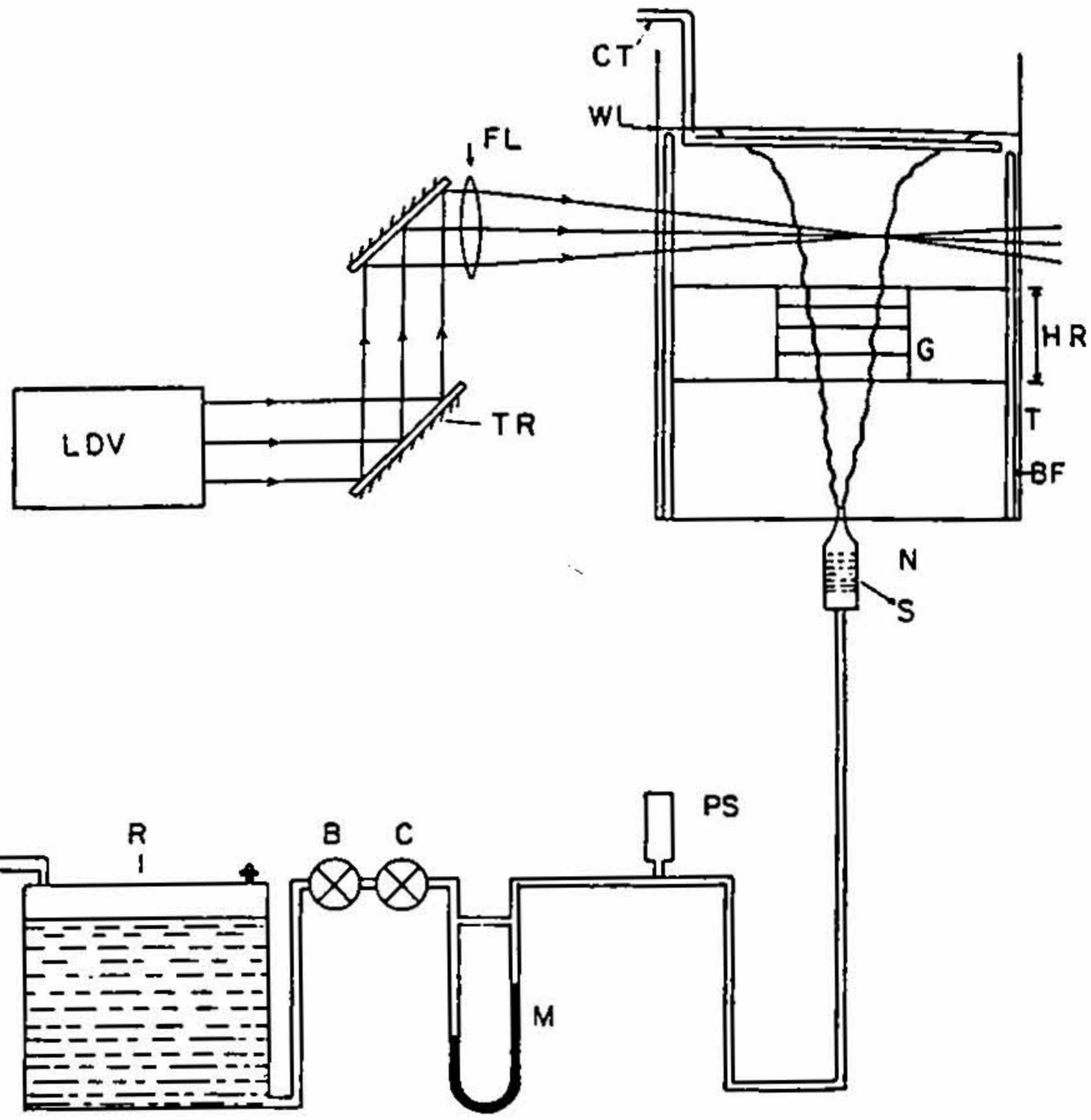

FIG. 1 Experimental arrangement.

The major portion of the work is experimental in nature and some attempts are also made to simulate the flow numerically.

2. Experimental set-up

A schematic of the experimental arrangement is shown in Fig. 1. The experiments are carried out in a glass tank (dimensions—60 × 60 × 120 cm (height)) filled with filtered and deionised water. The jet entered from the bottom of the tank through a stainless steel nozzle. The jet fluid, a mild solution of HCl with suitable amount of acetone added to make it neutrally buoyant with respect to the tank water, is supplied from a reservoir maintained at constant pressure. The volumetric heating of the jet fluid is achieved by the insertion of suitable electrodes made up of fine platinum wire (diameter = 0.09 mm) in the flow and application of high-frequency AC voltage across them. The high-frequency voltage is necessary to avoid the electrolysis of water. Since only the jet fluid conducts electricity, heating is localized and volumetric. In the present experiments, totally five electrodes are used, starting at 200 mm from the nozzle with a distance of 30 mm between them. The amount of heat input into the flow is controlled by controlling the current and voltage between the electrodes. The experiments are carried out for two different nozzle diameters (8 and 1.5 mm) and six different Reynolds numbers (ranging from 1360 to 3200—based on nozzle diameter and jet inlet velocity).

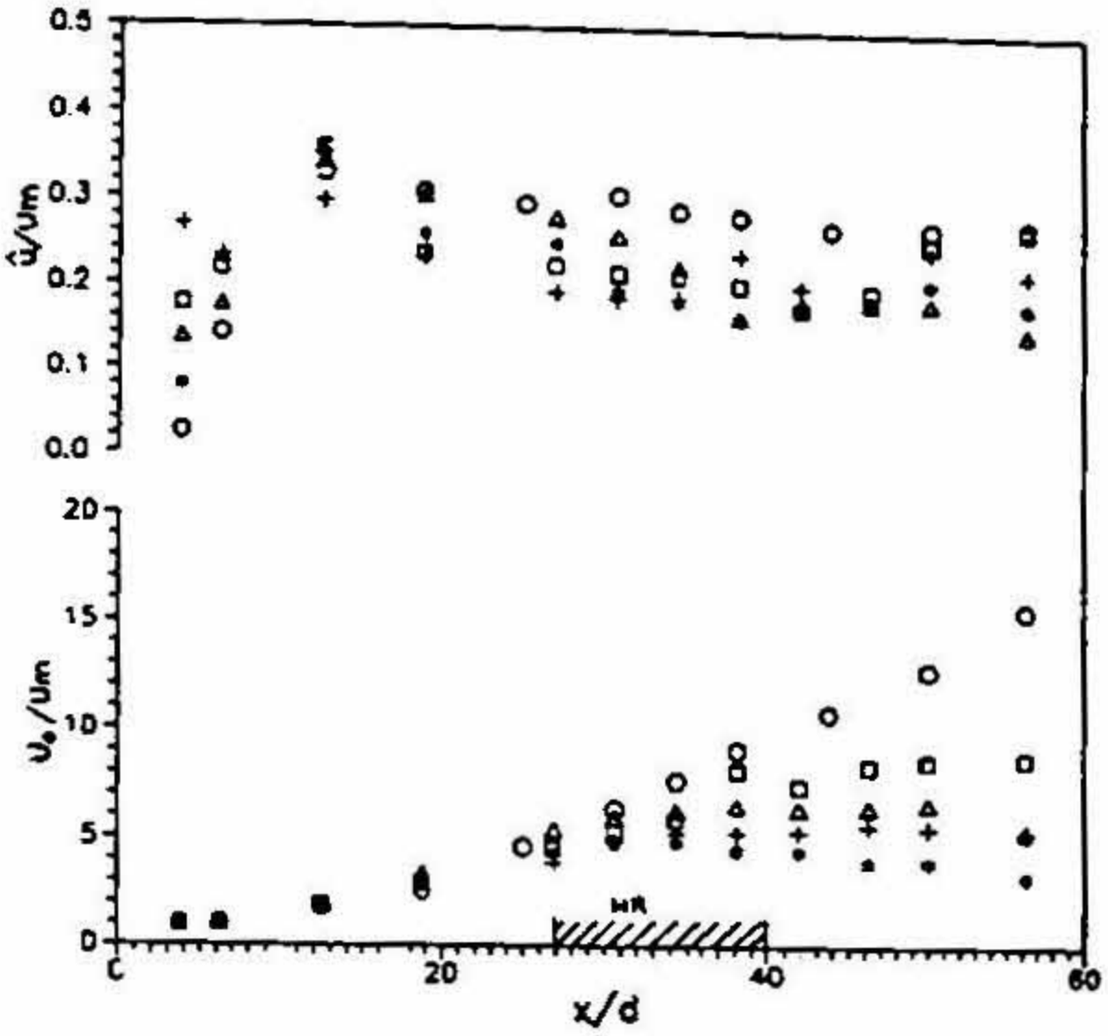

FIG. 2. Variation of axial component of velocity along the axis of the heated jet. Reynolds number = 1300. Nozzle diameter = 8 mm; HR = heated region; U_o – jet exit velocity; U_m – Centreline velocity; $\hat{u}$ – RMS value of fluctuating component of velocity; o – Unheated jet; – Q = 156 W; Δ – Q = 444 W; + – Q = 694 W; * – Q = 900 W.

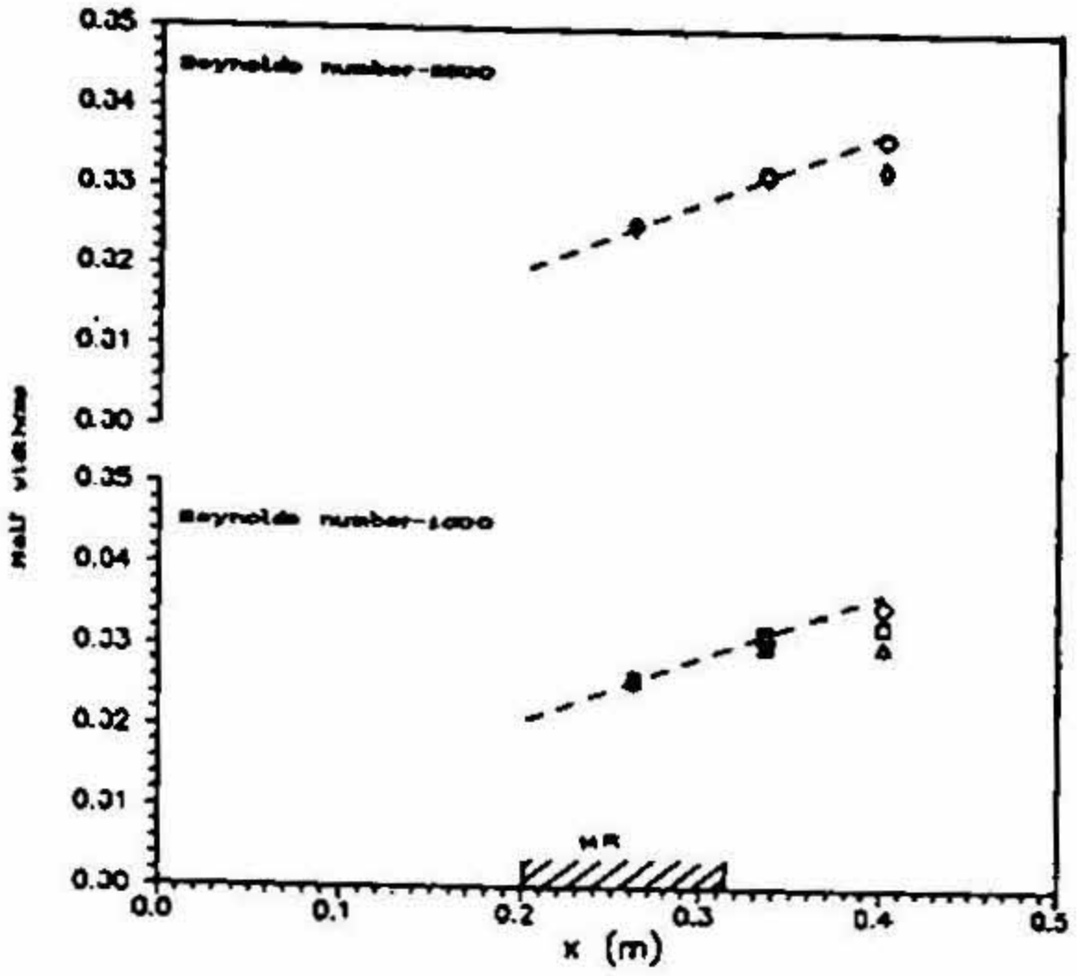

FIG. 3. Variation of the half-width in heated jet. Nozzle diameter = 1.5 mm. ——— – unheated jet; o – Q = 300 W; – Q = 500 W; Δ – Q = 750 W.

The flow is studied visually by laser-induced fluorescence technique. The presence of low velociti ·s, flow reversals and strong electric field ruled out the use of conventional hot wires for the vel· city measurements in the present study, and measurements of velocity field are carried out using laser Doppler velocimeter (LDV). The LDV used in the experiment is TSI, USA-supplied two-component back-scattered system.

3. Results

The unheated jet is initially studied before exploring the volumetrically heated jet. As a check on the entire arrangement, the unheated jet results are compared with the results from earlier studies and the agreement is found to be satisfactory.

Figure 2 shows the distribution of the normalized mean and the fluctuating velocity along the axis of the jet for heated and unheated jets. It is observed that the velocity decay rate is substantially reduced by the buoyancy enhancement and depending on heating rate (Q) there is a region over which velocity is almost constant. The normalized turbulent fluctuating velocity (normalized with the local maximum velocity) continues to decrease in the downstream direction. If the trend in the mean velocity is taken into account it turns out that the fluctuating velocity increases slightly. This suggests that the effect of buoyancy enhancement is more on the mean velocity field than that on fluctuating velocity.

Figure 3 shows the effect of buoyancy increase on the half-width of the jet. The flow visualization as well as the measurements indicate that the spread rate is reduced and at higher heating rates the jet even narrowed down slightly towards the top of the heat injection region. It was also observed that the characteristic recognizable large-scale eddies started disintegrating and disappearing as soon as they enter the heat-injection region. The mass flux across the jet

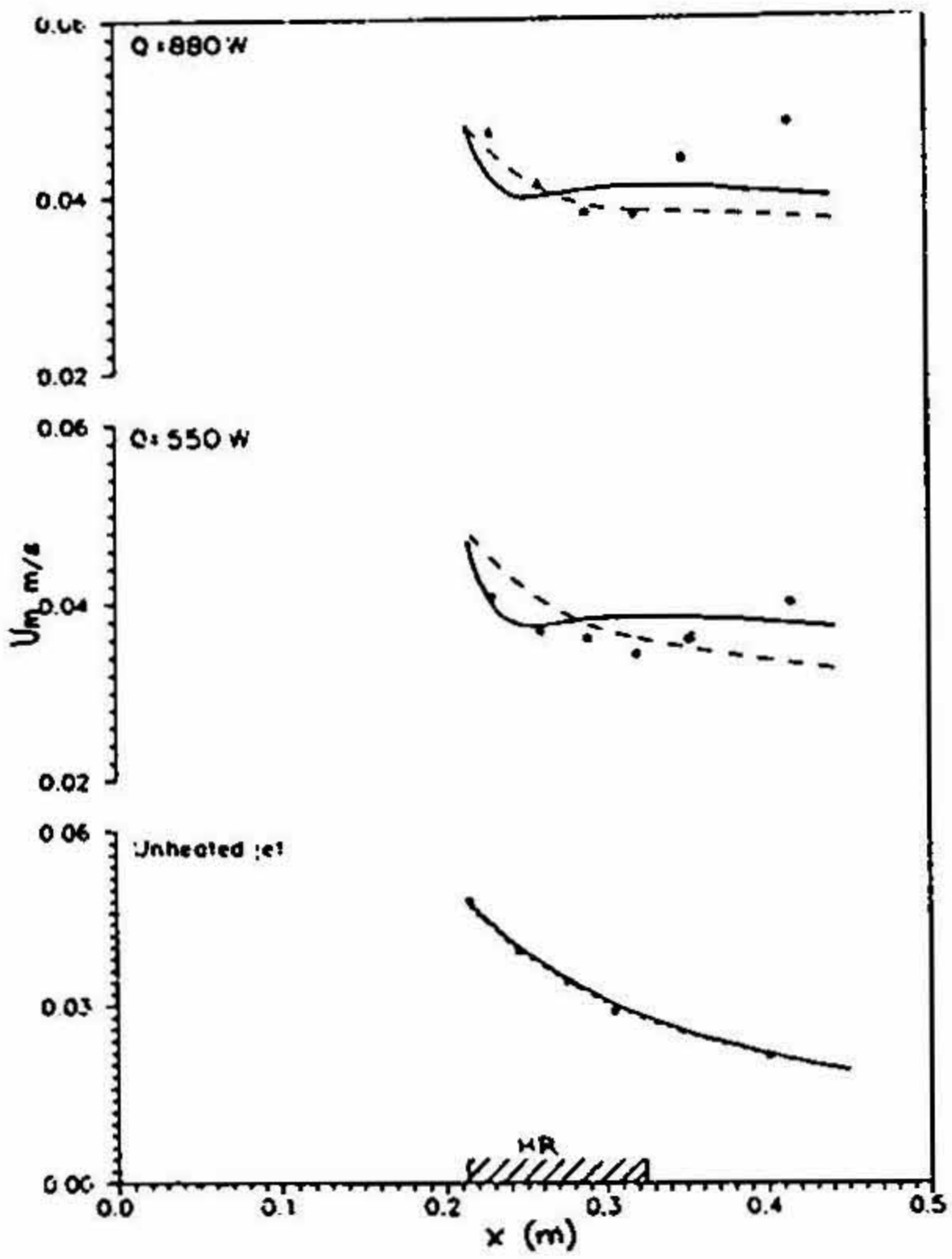

FIG. 4. Variation of axial component of velocity along the centreline. Reynolds number = 1300. Nozzle diameter = 8mm * – Experiment; ——— – Integral method; — – k-ε model.

shows an increase in the beginning of heat injection region but it became almost constant in the downstream.

The mean velocity distribution along the horizontal cross-section of the jet shows that the similarity in the mean velocity distribution is not noticeably affected by the buoyancy enhancement whereas it is disturbed in the fluctuating velocity field.

The centreline velocity and temperature and half-width have been calculated using an integral and differential models (K-ε model for turbulence). Both models predict the unheated jet behaviour with good accuracy; however, in the buoyancy-enhanced jet neither model can predict satisfactorily the velocity and spread rate, especially downstream of heat injection region (Fig. 4). This indicates that the effects of buoyancy enhancement on the turbulence structure are more subtle, and cannot be taken into account by the mere inclusion of buoyancy term in the governing equations.

4. Conclusions

The experimental results show that the structure and dynamics of the jet are considerably altered. The recognizable large eddies started disintegrating in the region of the buoyancy enhancement. The jet spread rate is reduced and become almost a constant diameter jet at high-heating rates. The mean axial component of velocity becomes more or less constant value at higher heat injec-

tion rates over some axial distance. The normalized fluctuating velocity decreased by a maximum of about 40% compared to the unheated jet. However, the non-normalized fluctuating velocity increased, but not as much as the mean. The similarity in the mean horizontal velocity profile is not altered by the buoyancy enhancement. The conventional approaches of modelling the flow are not very successful in predicting the flow development when volumetrically heated.

References

1. TURNER, J. S. — Model experiments relating to thermals with increasing buoyancy, *Q. J. R. Met. Soc.*, 1963, **89**, 62–74.

2. HERMANSON, J. C. AND DIMOTAKIS, P. E. — Effects of heat release in a turbulent, reacting shear layer, *J. Fluid. Mech.*, 1989, **199**, 333–375.

3. BHAT, G. S., NARASIMHA, R. AND ARAKERI, V. H. — A new method of producing local enhancement of buoyancy in liquid flows, *Expts Fluids*, 1989, 7, 99–102.